REPORT DOCUMENTATION PAGE

Form Approved OMB NO. 0704-0188

The public reporting burden for this collection of information is estimated to average 1 hour per response, including the time for reviewing instructions, searching existing data sources, gathering and maintaining the data needed, and completing and reviewing the collection of information. Send comments regarding this burden estimate or any other aspect of this collection of information, including suggesstions for reducing this burden, to Washington Headquarters Services, Directorate for Information Operations and Reports, 1215 Jefferson Davis Highway, Suite 1204, Arlington VA, 22202-4302. Respondents should be aware that notwithstanding any other provision of law, no person shall be subject to any oenalty for failing to comply with a collection of information if it does not display a currently valid OMB control number.
PLEASE DO NOT RETURN YOUR FORM TO THE ABOVE ADDRESS.

1. REPORT DATE (DD-MM-YYYY)	2. REPORT TYPE	3. DATES COVERED (From - To)
24-04-2015	MS Thesis	-

4. TITLE AND SUBTITLE

OFDM COUPLED COMPRESSIVE SENSING ALGORITHM FOR STEPPED-FREQUENCY GROUND PENETRATING RADAR

5a. CONTRACT NUMBER
W911NF-13-1-0301

5b. GRANT NUMBER

5c. PROGRAM ELEMENT NUMBER
611103

6. AUTHORS
Mohamed Metwally

5d. PROJECT NUMBER

5e. TASK NUMBER

5f. WORK UNIT NUMBER

7. PERFORMING ORGANIZATION NAMES AND ADDRESSES
University of Vermont
85 South Prospect Street, 340 Waterman Building
Burlington, VT 05405 -0160

8. PERFORMING ORGANIZATION REPORT NUMBER

9. SPONSORING/MONITORING AGENCY NAME(S) AND ADDRESS (ES)
U.S. Army Research Office
P.O. Box 12211
Research Triangle Park, NC 27709-2211

10. SPONSOR/MONITOR'S ACRONYM(S)
ARO

11. SPONSOR/MONITOR'S REPORT NUMBER(S)
63445-EL-RIP.3

12. DISTRIBUTION AVAILIBILITY STATEMENT
Approved for public release; distribution is unlimited.

13. SUPPLEMENTARY NOTES
The views, opinions and/or findings contained in this report are those of the author(s) and should not contrued as an official Department of the Army position, policy or decision, unless so designated by other documentation.

14. ABSTRACT

Dating back to as far as 1940, the US road and bridge infrastructure system has garnered quite the status for strategically connecting together half a continent. As monumental as the infrastructure's status, is its rate of deterioration, with the average bridge age coming at a disconcerting 50 years. Aside from visual inspection, a battery of non-destructive tests were developed to conduct structural fault assessment and detect laminations, in order to preemptively take preventive measures.
The mainstream commercially favored test is the impulse time domain ground penetrating radar (GPR). An

15. SUBJECT TERMS
OFDM, ground penetrating radar, compressive sensing

16. SECURITY CLASSIFICATION OF:			17. LIMITATION OF ABSTRACT	15. NUMBER OF PAGES	19a. NAME OF RESPONSIBLE PERSON
a. REPORT	b. ABSTRACT	c. THIS PAGE			Dryver Huston
UU	UU	UU	UU		19b. TELEPHONE NUMBER 802-656-1922

Report Title

OFDM COUPLED COMPRESSIVE SENSING ALGORITHM FOR STEPPED-FREQUENCY GROUND PENETRATING RADAR

ABSTRACT

Dating back to as far as 1940, the US road and bridge infrastructure system has garnered quite the status for strategically connecting together half a continent. As monumental as the infrastructure's status, is its rate of deterioration, with the average bridge age coming at a disconcerting 50 years. Aside from visual inspection, a battery of non-destructive tests were developed to conduct structural fault assessment and detect laminations, in order to preemptively take preventive measures.

The mainstream commercially favored test is the impulse time domain ground penetrating radar (GPR). An extremely short, high voltage pulse is used to visualize cross-sections of the bridge decks. While effective and it does not disturb traffic flow, impulse radar suffers from major drawbacks. The drawbacks are namely, its limited dynamic range and high cost of system manufacturing. A less prominent yet highly effective system, stepped frequency continuous wave (SFCW) GPR, was developed to address the aforementioned drawbacks. Mostly developed for research centers and academia, SFCW boasts a high dynamic range and low cost of system manufacturing, while producing comparable if not identical results to the impulse counterpart. However, data procurement speed is an inherent problem in SFCW GPR, which seems to keep impulse radar in the lead for production and development.

I am proposing a novel approach to elevate SFCW's data acquisition speed and its scanning efficiency altogether. This approach combines an encoding method called orthogonal frequency division multiplexing (OFDM) and an emerging paradigm called compressive sensing (CS). In OFDM, a digital data stream, the transmit signal, is encoded on multiple carrier frequencies. These frequencies are combined in such a way to achieve orthogonality between the carrier frequencies, while mitigating any interference between said frequencies. In CS, a signal can be potentially reconstructed from a few samples below the standardized Nyquist rate. A novel design of the SFCW GPR architecture coupled with the OFDM-CS algorithm is proposed and evaluated using ideal channels and realistically modelled bridge decks.

OFDM COUPLED COMPRESSIVE SENSING ALGORITHM FOR STEPPED-FREQUENCY GROUND PENETRATING RADAR

A Thesis Presented

by

Mohamed Metwally

to

The Faculty of the Graduate College

of

The University of Vermont

In Partial Fulfillment of the Requirements
for the Degree of Master of Science
Specializing in Electrical Engineering

Oct, 2014

Accepted by the Faculty of the Graduate College, The University of Vermont, in partial fulfillment of the requirements for the degree of Master of Science, specializing in Electrical Engineering.

Thesis Examination Committee:

_____ Advisor
Dr. Tian Xia, Ph.D.

_____ Committee Member
Dr. Gagan Mirchandani, Ph.D

_____ Chairperson
Dr. Dryver Huston, Ph. D.

_____ Dean, Graduate College
Dr. Cynthia J. Forehand, Ph.D.

Date: June 13th, 2014

ABSTRACT

Dating back to as far as 1940, the US road and bridge infrastructure system has garnered quite the status for strategically connecting together half a continent. As monumental as the infrastructure's status, is its rate of deterioration, with the average bridge age coming at a disconcerting 50 years. Aside from visual inspection, a battery of non-destructive tests were developed to conduct structural fault assessment and detect laminations, in order to preemptively take preventive measures.

The mainstream commercially favored test is the impulse time domain ground penetrating radar (GPR). An extremely short, high voltage pulse is used to visualize cross-sections of the bridge decks. While effective and it does not disturb traffic flow, impulse radar suffers from major drawbacks. The drawbacks are namely, its limited dynamic range and high cost of system manufacturing. A less prominent yet highly effective system, stepped frequency continuous wave (SFCW) GPR, was developed to address the aforementioned drawbacks. Mostly developed for research centers and academia, SFCW boasts a high dynamic range and low cost of system manufacturing, while producing comparable if not identical results to the impulse counterpart. However, data procurement speed is an inherent problem in SFCW GPR, which seems to keep impulse radar in the lead for production and development.

I am proposing a novel approach to elevate SFCW's data acquisition speed and its scanning efficiency altogether. This approach combines an encoding method called orthogonal frequency division multiplexing (OFDM) and an emerging paradigm called compressive sensing (CS). In OFDM, a digital data stream, the transmit signal, is encoded on multiple carrier frequencies. These frequencies are combined in such a way to achieve orthogonality between the carrier frequencies, while mitigating any interference between said frequencies. In CS, a signal can be potentially reconstructed from a few samples below the standardized Nyquist rate. A novel design of the SFCW GPR architecture coupled with the OFDM-CS algorithm is proposed and evaluated using ideal channels and realistically modelled bridge decks.

ACKNOWLEDGEMENTS

CITATIONS

Material from this thesis is being prepared with the intent of publishing.

Chapter 2 is a paper intended for journal publication in the Journal of Electronic Testing: Theory and Applications.

Similarly, Chapter 3 is a paper intended for journal publication in the IEEE Geoscience and Remote Sensing Journal.

TABLE OF CONTENTS

Page

LIST OF TABLES

Table Page

LIST OF FIGURES

Figure Page

CHAPTER 1: LITERATURE REVIEW

1.1. Establishing Problem Scenario

The United States contains a road network dating to 1940 with more than 570,000 bridges in service, of which nearly 368,000 have concrete decks [1]. With 3.8 trillion vehicle-kilometers per year, the US roadway infrastructure is considered to be one of the largest in the world [10]. Heavy usage has contributed to the deterioration of the infrastructure at a rapid rate. The average interstate bridge is roughly 40 years old while most bridges are more than 50 years of age [10]. There exists a national bridge inspection program to discover structurally inadequate bridges and yet it is not effective.

Structural faults and distress within roadway infrastructure are noticed underneath the surface and no visual inspection can account for these types of faults. In fact, if a fault is detectable visually then the structure has already been compromised too much for safe operation by the public. The majority of the maintenance funds for these bridges are mostly spent on the highly compromised bridges. However, a more successful approach is to adopt a preventive measure such as periodic testing for bridge decks. These tests would detect any faults early on and establish a time frame for when the bridge would need maintenance or renovating.

1.2. Ground Penetrating Radar History and Applications

In 1910, a German patent by Leimback and Lowy claimed the first recorded use of electromagnetic waves to locate buried objects. A circular arrangement of vertical bore-holes containing dipole antennas was employed. Electromagnetic waves were transmitted between adjacent pairs of antennas and the magnitudes of continuous wave electromagnetic

reflections from ground were compared. This resulted in an approximate image of the ground's dielectric properties[2][3]. Nineteen years later, German geophysicist W. Stern recorded the first GPR measurement of a glacier's depth in Austria. The technology was originally built for the military to detect landmines and was used extensively in lunar investigations in early 1970s. After 1970, GPR's applications diversified widely [9] to the following areas:

- Archaeology and locating hidden sites
- Bridge deck analysis
- Borehole inspection
- Building structural fault assessment
- Contaminated land assessments
- Detection of buried war mines – both anti-personal and anti-tank
- Evaluating structurally integrity of reinforced concrete
- Forensic investigations
- Medical imaging
- Pipes and cable detection for city planning
- Inter-planetary exploration
- Tunnel linings

In general principle, ground penetrating radar radiates electromagnetic waves through ground and records the reflections or echoes from the ground. The analysis of this information allows the user to remotely sense what is underground. Sheers' Figure 1 below illustrates a generic GPR model.

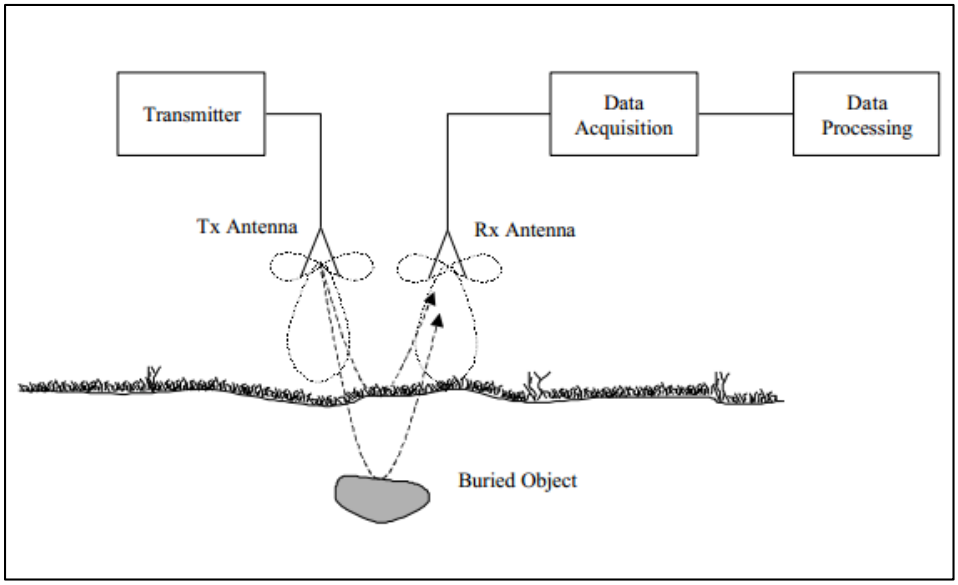

Figure 1 Generic Model for Ground Penetrating Radar [8]

A number of factors which are all frequency dependent, constitute how different materials and objects reflect the electromagnetic waves. These factors are material attributes, namely, permittivity ε, conductivity σ and magnetic permeability μ. The disparity of permittivity between different materials underground brings about the distinct reflections to any incoming electromagnetic waves. Conductivity is responsible for how much of the radiated signal gets absorbed or reflected by the medium. Radar applications mostly deal with materials that are native to Earth, hence mostly non-magnetic. This means that there is very little contribution by the magnetic permeability factor. After the reflections are analyzed, different dimensional scans can be formed to visualize the structure underground. In the case of 1-D, it is called an A-scan as illustrated in Scheers' Figure 2 below. A horizontal collection of A-scans ensemble forms a 2-D image called a B-Scan.

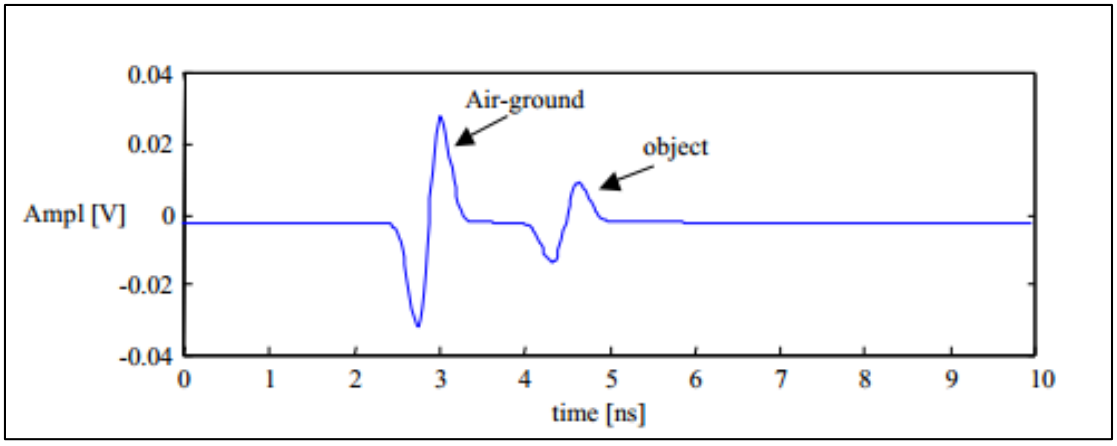

Figure 2 A-scan accompanying the aforementioned generic model [8]

After 1970, the general public started to see its potential in non-destructive testing of structures and in satellite remote sensing [2].

1.3. Existing Solutions – Non-Destructive Testing Methods

An array of non-destructive testing methods have been developed over the past two decades that are applicable for bridge deck inspection and fault detection. These methods include linear polarization techniques for corrosion assessment, chain drag test, impact echo, infrared tomography and ground penetrating radar.

The chain drag method is the most simplistic, execution wise, of the aforementioned methods. The method involves dragging a heavy metal chain across the bridge deck and recording or listening to the acoustic response from the concrete deck. A structurally sound bridge deck produces an acoustic response that is set as the baseline for comparison by the operator. Any area within the concrete bridge deck that has developed structural faults or delaminations will produce a distinct acoustic response differing than that of the baseline. This testing method is however limited to delaminations that are large enough for detection. This means that any potential delaminations still developing will not

be registered during the test. In addition, it is heavily dependent on a qualitative metric, namely the operator's hearing, to indicate the structural soundness of the bridge deck. Furthermore, it is not an effective method if the bridge deck happens to have been coated with a hot-mix asphalt (HMA) overlay. Loulizi's Table 1 indicates a comparison between the different NDE methods used for bridge inspection commercially.

	VI	LP	HCP	CD	IE	UT	IR	AE	GPR
Does HMA overlay need to be removed?	No	Yes	Yes	Yes	No	Yes	No	No	No
Does road or bridge need to be closed?	Yes	Yes	Yes	Yes	Yes	Yes	No	Yes	No
Testing duration	Long	Very Long	Very Long	Long	Very Long	Long	Fast	Long	Fast
Testing speed (km/h)	N/A	N/A	N/A	N/A	N/A	N/A	80	N/A	80
Penetration depth (mm)	0	50	50	50	300	50	100	300	300-2000*
Temperature limitation	No	No	No	No	No	No	Yes	No	No

VI: Visual Inspection LP: Linear Polarization HCP: Half Cell Potential
CD: Chain Drag IE: Impact Echo UT: Ultrasonic
IR: Infrared Thermography AE: Acoustic Emission GPR: Ground Penetrating Radar
* Depends on structural material and frequency of operation

Table 1 Comparison between NDE methods used for bridge inspection

The literature review will focus on the different types of ground penetrating radar (GPR) techniques and their drawbacks. GPR employs approaches that operate in both time and frequency domains as illustrated in Figure 3 below.

1.4. Types of Ground Penetrating Radar Systems

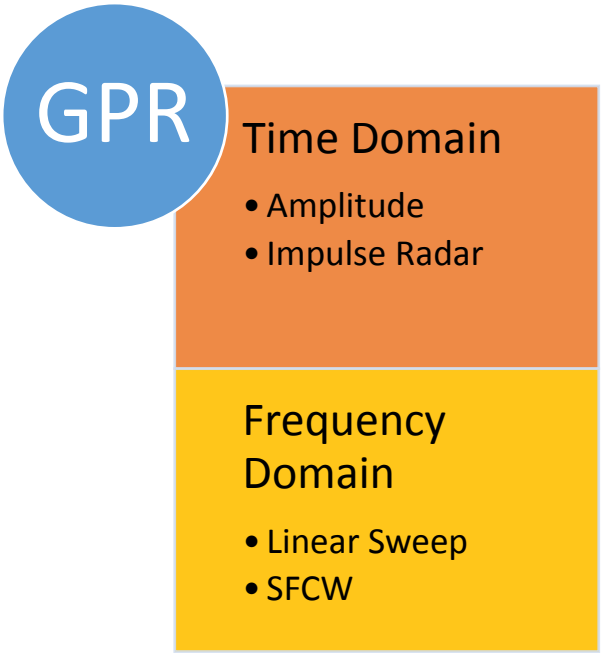

Figure 3 Different Types of Ground Penetrating Radar

1.4.1. Amplitude Modulated Time Domain

Starting with the time domain methodologies is the amplitude modulated technique. Using circuitry based on avalanche transistors or Step Recovery Diodes (SRD) coupled with Marx generators, an extremely short pulse with high amplitude is generated and formed into a monocycle as illustrated below in Frank Sabbath's figure. This pulse is used to modulate a carrier frequency before transmission into the channel. A monocycle shape is optimally used since it provides the shortest pulse duration allowing for a larger range resolution. It is important to note that the 3dB bandwidth of the transmitted pulse is equal to the center frequency of the transmitted pulse.

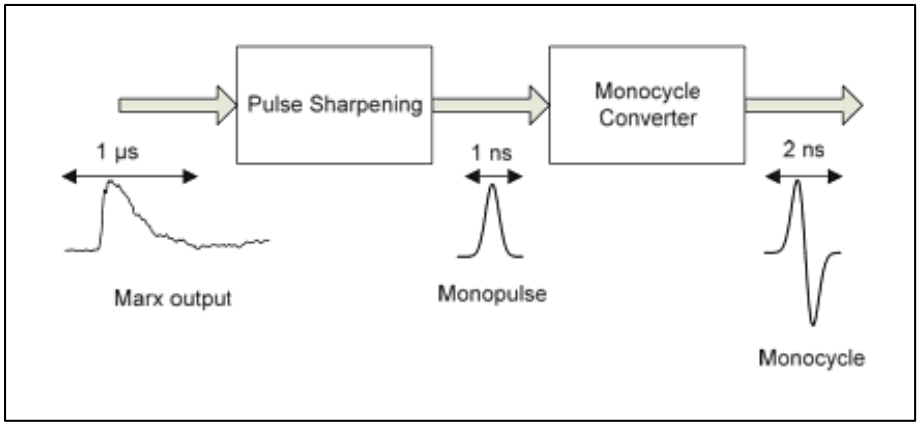

Figure 4 Generic block diagram for generating a monocycle

1.4.2. Impulse Radar

To overcome the bandwidth limitation posed by the amplitude modulation technique, the impulse radar was developed. An impulse radar is known by many terms such as non-sinusoidal, carrierless, baseband or time domain radar. The transmitted pulse is distinct in that it has no carrier frequency. The pulse width can vary from the order of a few nanoseconds to a few hundred picoseconds. These pulse widths cover a very wide bandwidth in the frequency spectrum. Hence, impulse radar is under ultra-wide bandwidth classification of radars. A radar system is defined by the Defense Advanced Research Project Agency [4] to be UWB if its fractional bandwidth is larger than 25%. Furthermore, a system's fractional bandwidth can be calculated as follows:

$$B_{fractional} = 2 * (f_{max} - f_{min}) * \ 100\%$$

f_{max} & f_{min} are the highest and lowest frequency respectively covered within the operational range. The operational range is usually where 95% to 99% of the signal's power lies. Figure 5 and Figure 6 [9] illustrate a generic model for an impulse radar system and a block diagram for a more detailed impulse radar.

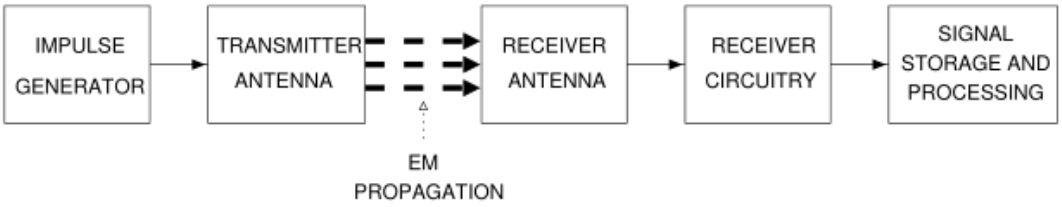

Figure 5 Generic block diagram for impulse radar [5]

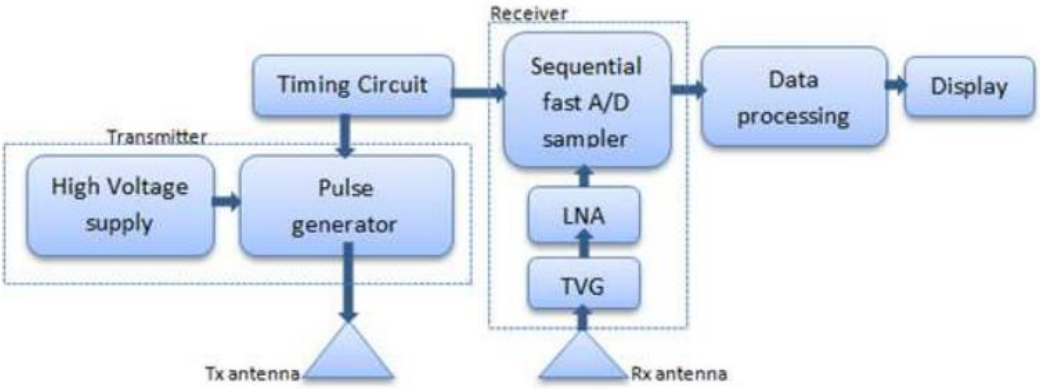

Figure 6 Detailed block diagram for an impulse radar system [9]

The impulse generator is one of the most distinctive components in the impulse radar architecture, responsible for generating non-sinusoidal pulses. These pulses have very high amplitudes and extremely short pulse widths. Such pulses are possible with the help of a low impedance, a quick rise time and high voltage. Pulse durations are typically between 0.6ns to 10ns per the impulse radar application [5]. The high amplitudes reaching sometimes thousands of volts are typically made possible using Marx banks shown in Figure 7. Marx banks are storage devices that are charged in parallel and discharged in series [6]. A system is designed with X number of stages. Every stage will have a charging impedance such as a resistor or inductor to charge a capacitor. Every bank in each of the X

stages will have a switch. Simultaneously, all the switches are closed to create a series connection between all the charged X capacitors. Hence, the voltage output (discharge in series) is a large multiple of the stored charge across the different storage capacitors (stages) [6].

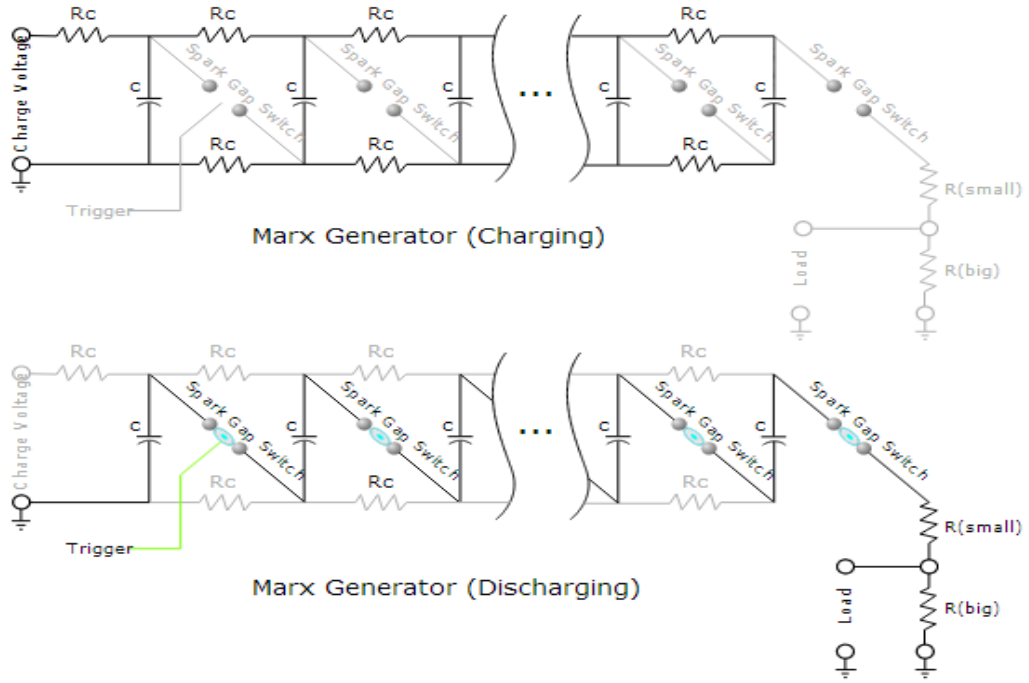

Figure 7 Marx Generator with spark gap switches

While impulse radar offers a solution to the bandwidth problem, fast scan times and an easy architecture to implement, it has several drawbacks. Firstly, the bandwidth usage dictates the need for an extremely fast Analog-to-Digital converter which are very expensive components. In addition, the impulse radar system suffers from limited dynamic range. Dynamic range is the difference between the maximum detectable signal power that the system can tolerate without distortion and the minimum detectable signal power. The coverage of very wide bandwidths in frequency spectrum makes it difficult to filter out the

noise from the reflections. Hence, more power needs to be supplied to the transmitted signal to better isolate the noise. Adding too much power would saturate the components in the receiver circuitry as well and so the radar operates in a limited dynamic range.

Even though the majority of commercial GPRs are time domain based, there have been several GPRs developed in the frequency domain in academia and research centers. The frequency domain mainly utilizes two continuous wave approaches; linear sweep and stepped frequency continuous wave radar.

1.4.3. Frequency Modulated Continuous Wave GPR

The linear sweep also called the frequency modulated continuous wave (FMCW). Figure 8 shows a block diagram for a FMCW radar system [8]. It transmits a continuous wave with a continuously changing carrier frequency using a voltage controlled oscillator (VCO). Given a certain dwell time, the VCO linearly sweeps a specified frequency range using a saw tooth, sine, square or triangular function. The reflections are mixed with the transmitted wave. The difference in frequencies between the two waves is a function of the depth of the target.

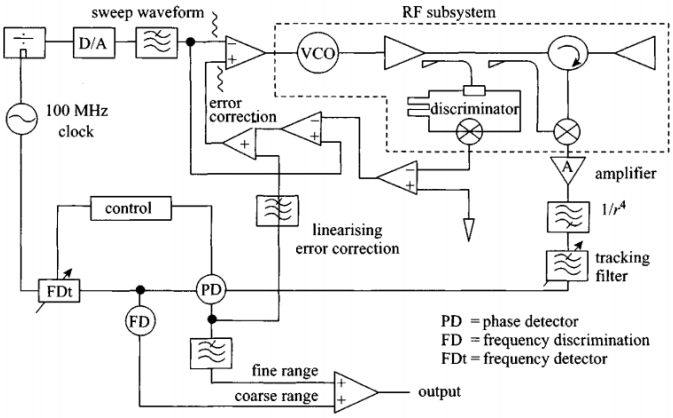

Figure 8 Detailed block diagram of FMCW radar [8]

The following equations illustrate how to determine the target depth using a linear sweep triggered by a saw tooth waveform:

$$k = \frac{\Delta f_{radar}}{\Delta t_{radar}}$$

where f_{radar} is the entire frequency range being swept within a certain time t_{radar}.

To calculate the round trip time to receive the reflections:

$$t_{roundtrip} = \frac{\Delta f_{echo}}{k}$$

where Δf_{echo} is the difference between the transmitted and received frequency.

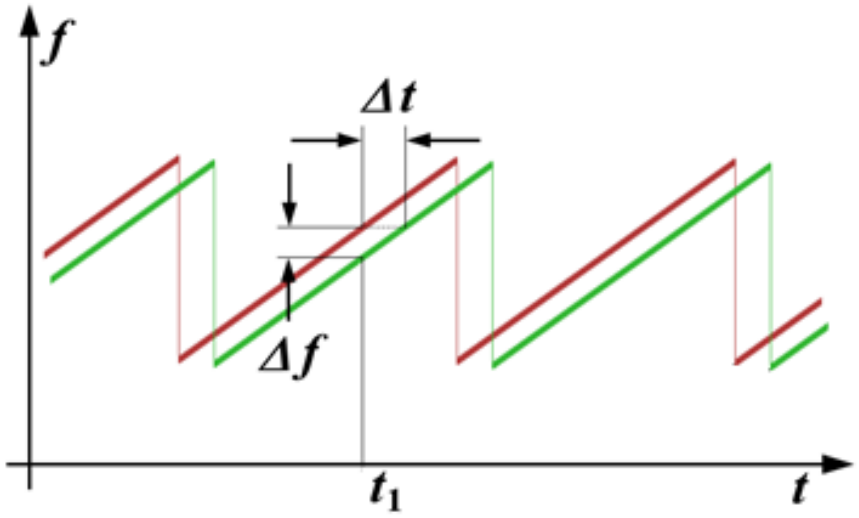

Figure 9 Transmitted (red) and received (green) FMCW signals

$$Operational\ Range = \frac{Speed\ of\ light}{(4\ x\ Modulation\ Frequency}$$

Finally, to calculate the target depth:

$$distance_{target} = \frac{c' t_r}{2}$$

$$c' = \frac{c}{n}$$

where c is the speed of light and n is the refractive index of medium. On the other hand, FMCW suffers from restricted dynamic range as well since it is receiving signals while transmitting simultaneously. This results in direct coupling between transmitter and receiver antennas which could mask the smaller weaker reflections from ground.

1.4.4. Stepped Frequency Continuous Wave GPR

To address both the bandwidth issue posed by amplitude modulated time domain GPR and the limited dynamic range posed by both impulse radar and FMCW, stepped frequency continuous wave (SFCW) GPR was developed. A block diagram illustrating the general operations carried out by SFCW is seen in Figure 10 [7].

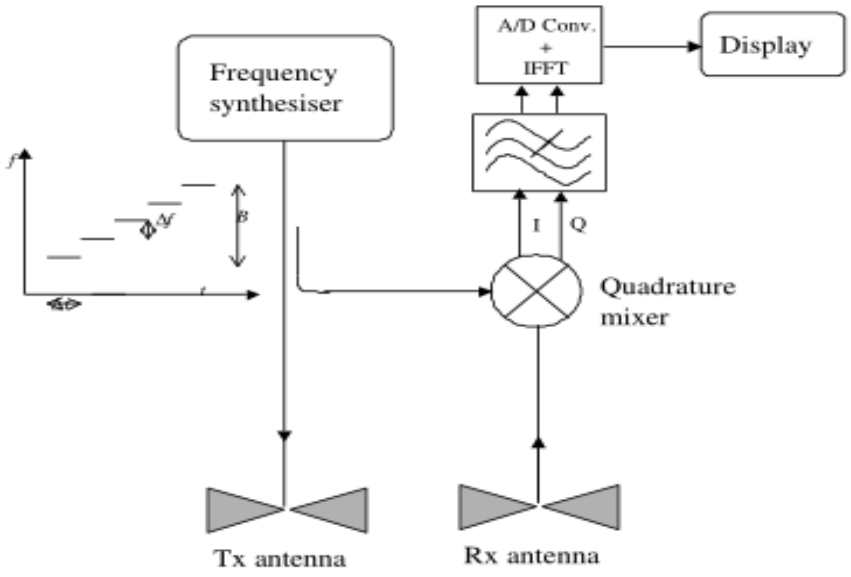

Figure 10 General block diagram for SFCW radar [7]

SFCW utilizes continuous sinusoidal waves of different frequencies to create synthetic range profiles. During each measurement, a single frequency sinusoid is transmitted, received and analyzed for gain and phase difference values. This approach greatly simplifies the generation, reception and digitization involved. A frequency synthesizer steps through a range of frequencies equally spaced by a certain Δf and a corresponding continuous sinusoid is radiated [8]. The reflected echoes are mixed with the emitted wave using a quadrature mixer. The mixer outputs I (real) and Q (imaginary) components of the baseband signal. With the signal in baseband, cheap, high precision and low speed Analog-to-Digital converters can be used to sample I and Q signals. For each frequency, the gain and phase is calculated using the corresponding transmitted and received waves for the particular frequency. The gain and phase values are all assembled in a matrix and passed through the Inverse Fast Fourier Transform to produce the time domain representation of the targets' reflections.

The phase of the returning echoes is used for range determination, but practically, a series of stepped frequencies are needed to obtain practical operational ranges. The following equations [7] will demonstrate this. Consider the emitted signal at frequency f_1.

$$Emitted = Acos(2\pi f_1 t)$$

The reflected signal from a target at a particular depth R is

$$Received = A_{received}\cos(2\pi f_1 t + \theta)$$

where the phase θ is equated to the frequency f_1 and the time taken to get the reflection back:

$$\theta = 2\pi f_1 t_{reflection} = 2\pi f_1 \left(\frac{2R}{c}\right)$$

where c is the speed of light. Hence solving for the depth R, we get:

$$R = \frac{c}{f_1}\frac{\theta}{4\pi} = \frac{\lambda}{4\pi}\theta$$

and λ is the wavelength. Hence, by observing the equation, the maximum unambiguous range occurs when $\theta = 2\pi$. A target's depth can be determined accurately if it falls within the unambiguous range. For radars that only depend on one frequency, it is highly impractical for target detection since the unambiguous range is very small. For example, a 1GHz transmit frequency produces the following range:

$$R = \frac{3x10^8 m/s}{1x10^9 1/s}\frac{2\pi}{4\pi} = \frac{3x10^8 m/s}{2x1x10^9} = 15cm$$

Using SFCW, enables us to use multiple frequencies to synthesize the target range profile. Consider a radar that employs two frequencies, f_1 and f_2.

$$Emitted_1 = A_1\cos(2\pi f_1 t) \;\; \& \;\; Emitted_2 = A_2\cos(2\pi f_2 t)$$

The reflected signal from a target at a particular depth R is

$$Received_1 = A_{r1}\cos(2\pi f_1 t + \theta_1) \;\; \& \;\; Received_1 = A_{r2}\cos(2\pi f_2 t + \theta_2)$$

And the phase difference is calculated between the two target reflections as follows:

$$\Delta\theta = \theta_2 - \theta_1 = \frac{4\pi R}{c}(f_2 - f_1)$$

To solve for R,

$$Unambiguous\ Range = \frac{c\Delta\theta}{4\pi\Delta f}$$

To obtain the maximum unambiguous range, the phase difference is set to 2π.

$$Unambiguous\ Range = \frac{c}{2\Delta f}$$

And the range resolution is determined using the overall system bandwidth. For an SFCW system with n steps with a frequency step size Δf.

$$Range\ Resolution = \frac{c}{2n\Delta f}$$

For a SFCW system with 100 steps spanning between 1GHz and 2GHz, the step size is 10 MHz, and the range resolution is:

$$Range\ Resolution = \frac{3x10^8 m/s}{2x(100)x(10x10^6)s^{-1}} = 0.15\ meters$$

$$Maximum\ Unambiguous\ Range = \frac{3x10^8 m/s}{2x(10x10^6)s^{-1}} = 15\ meters$$

Hence, using multiple frequencies such as in the SFCW radar case, one can achieve a more useful maximum unambiguous range.

The stepped frequency GPR has several advantages over its time domain GPR counterpart. It can be designed with a greater dynamic range with the help of a narrowband coherent receiver and narrowband filters. In addition, between a time domain GPR system and a stepped frequency GPR with the same bandwidth, the stepped frequency GPR will produce much higher Signal-to-Noise ratio [7]. The high SNR is due to SFCW having a much higher mean radiated power when compared to the time domain GPR. On the other hand, SFCW has to sequentially step through each frequency for a range of frequencies and then assemble the analyzed responses to create one A-scan. This sequential stepping combined with assembling several A-scans is time-consuming and impractical if a bridge deck is to be scanned without interrupting traffic flow or closing the bridge down.

1.5. Proposed Approach

Stepped frequency GPR addresses the bandwidth and the dynamic range problems. In addition, it is cheaper to realize hardware wise since the sampling is performed on baseband signals. Its major drawback is the length of time needed to complete a single scan. I propose to incorporate two techniques to drastically reduce the time needed to complete the A-scan. The method encompasses integrating Orthogonal Frequency Division Multiplexing (OFDM) coupled with compressive sampling to the existing SFCW GPR architecture. OFDM equips the SFCW GPR to send multiple individual frequencies simultaneously using the orthogonality feature. Instead of stepping through every frequency sequentially, the specified bandwidth is split into sub bands and each band is transmitted at once.

Compressive sensing is a novel way of analyzing a signal by the information it carries instead of its metrics such as bandwidth. By transforming the signal to a domain (frequency domain) where the signal is represented by few dominant coefficients, the signal gets compressed. The compression of the aforementioned signal discards the small coefficients or frequencies in this case. Reducing the number of frequencies that need to be transmitted contributes to the reduction in scan time without losing any significant information from the A-scan.

CHAPTER 2: COMPRESSIVE SAMPLING COUPLED OFDM TECHNIQUE FOR TESTING CONTINUOUS WAVE RADAR

2.1. Abstract

Testing radar circuitry is a challenging and time consuming process which requires characterizing system response over a wide range of frequencies. Radar circuitry is tested mainly through the functional test, where step frequency continuous wave (SFCW) is the primary method adopted. SFCW systems must generate and test a large number of frequencies. For an ultra-wideband radar system, testing circuitry with SFCW can be very time consuming. In this paper, we propose a new methodology to increase test speed with low cost and low design overhead by combining OFDM (Orthogonal Frequency Division Multiplexing) in conjunction with compressive sampling (CS) algorithms. OFDM makes it possible to generate and test multiple frequencies simultaneously, reducing test time. Additionally, compressive sampling techniques reduce the total amount of frequencies to be tested, further accelerating test speed and power consumption. To show equivalent performance between testing methods, SFCW and OFDM coupled CS techniques are all applied to characterize a simulated ground channel.

2.2. Introduction

Radio detection and ranging (radar) systems allow detection and ranging of objects at a distance, opening them to a vast array of different applications. Radar systems work by transmitting a signal through a medium, and measuring characteristics of the back-scattering signal. Typical characteristics measured include magnitude phase variations.

There are two common types of radar systems, which are impulse radar and continuous wave (CW) radar. Impulse radar operates by transmitting a pulse signal, and characterizing the reflection response. Typically, the pulse transmitted is very narrow in the time domain, which occupies a wide bandwidth in the frequency domain. The returning signal must then be received, sampled, and analyzed. In order to capture the response signal, very high speed A/D converter is required. The requirement of high speed ADC hardware is a major drawback, as it greatly increases the cost of the design.

A main alternative to the impulse architecture is CW radar. Stepped frequency continuous wave (SFCW) radar is one of the most common type of CW radar. Rather than emitting a pulse signal, SFCW systems send many individual frequency tones independently, and then measure each tone's phase and amplitude responses. Since a pulse signal can be decomposed into a series of individual frequency components, SFCW techniques can be used to synthesize a pulse signal transmitted over the device or channel. SFCW radar has many advantages over impulse radar system. First, implementations of SFCW architecture do not require expensive ADC circuitry as impulse systems use. Additionally, at each frequency, SFCW system operates in a narrowband mode, which allows higher transmitted power per frequency tone, and thus leads to higher dynamic range. However SFCW does face one primary drawback: each individual frequency tone must be generated, transmitted, and received sequential, resulting in longer SFCW operation than its impulse counterpart.

CW radar testing is typically performed using SFCW method, where radar system performance is characterized at each frequency sequentially. In order to generate

frequencies over a wide operational bandwidth, phased-locked loops (PLL) are commonly employed. PLLs can adjust their output divider incrementally to sweep frequencies sequentially. However, due to the time it takes to switch frequencies, the functional test faces the same drawback of long test time. Improvements can be made to SFCW test methods by generating or testing multiple frequency tones simultaneously. A common approach utilizes multiple phase locked loops to simultaneously generate frequencies, reducing the inactive time waiting for a PLL to lock into a frequency tone. Using multiple PLLs have the shortcoming of significantly increasing the cost and complexity of the design [1], [2]. Designs utilizing one or more PLL circuits are still slow test methods, with the test duration increasing for larger operational bandwidths. Some test circuits employ Arbitrary Waveform Generators (AWG) [3], [4]. AWGs can be programmed to create signals containing various desired frequencies and phases, and are often used for production tests and characterization. However, a traditional AWG requires very high frequency circuitry and a considerable amount of memory for data pattern storage As a result, AWGs can cost over $10,000. Due to the expense and cumbersome nature of AWGs, often they cannot be employed in testing. An alternative method which is implemented using an FPGA and a high speed DAC was proposed in an earlier publication [5]. The method proposed incorporates Orthogonal Frequency Division Multiplexing (OFDM) and the application of compressive sensing (CS) theory. OFDM allows multiple frequencies to be tested simultaneously. By transmitting multiple frequencies at a single time, test times can be reduced proportionally. Equivalence between the functional SFCW test method and OFDM test method was shown in previous work [5]. CS allows a reduction in the number

of test frequencies by exploiting the sparsity of a frequency response. Reconstruction algorithms can be used on an incomplete signal to generate the full frequency response. By combining OFDM and CS methods, testing times can be significantly improved, with less output power required.

This paper is organized as follows. Section II presents the technical explanation of OFDM. Following this, Section III explains the theory behind compressive sampling. Section IV explains the testing methodology, followed with our results. Section V introduces a proposed hardware testing architecture, and Section VI contains concluding remarks.

2.3. Orthogonal Frequency Division Multiplexing

OFDM techniques allow the transmission of multiple individual frequency tones simultaneously. By transmitting frequencies that are orthogonal to one another, cross-talk between frequency tones is mitigated. Orthogonality requires that the sub-bands are spaced at

$$Fa = \frac{k}{Ts}$$

Ts is the OFDM symbol period, and k is any integer. For simplicity, a k value of 1 is selected. Figure 1 below shows the frequency spectrum of an N-tone OFDM signal, with bandwidth Rs and frequency spacing Fa. The total signal bandwidth is $Rs = N * Fa$.

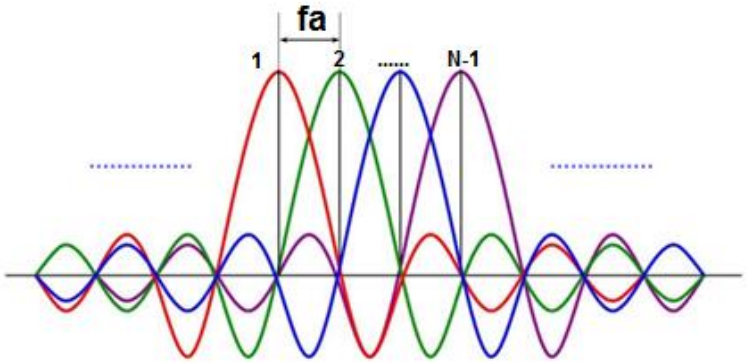

Figure 11 Frequency spectrum of N-tone OFDM signal

For OFDM symbol generation, a square wave spectrum with constant amplitude and phase can be employed for multi-tone signal generation. However, there is a significant drawback in that the inverse FFT of a square wave spectrum produces a sinc function in time domain, wherein except the data points on the main lobe, all others have small values. Due to noise, any information not contained in the main lobe could be lost or corrupted due to a low signal to noise ratio. Alternatively, the implementation utilizes the 4-QAM (QPSK) scheme, where symbol amplitudes are randomly assigned to ±1±1j for the real and imaginary components [6, 7]. As a result, all frequency components have a phase of -$\frac{3\pi}{4}$, -$\frac{\pi}{4}$, $\frac{\pi}{4}$, or $\frac{3\pi}{4}$. Upon IFFT, the time domain signals have relatively higher amplitudes and higher signal to noise ratio, which can alleviate the noise impact and, hence, improve test accuracy. The generated OFDM signal can be up-converted if necessary, and transmitted through the medium or DUT. Once the signal response is received, it must be sampled by ADC hardware. If the signal was upconverted, it may be necessary to down convert the signal to baseband before sampling. The sampled signal is then passed through

an FFT algorithm to return the signal to the frequency domain. Once in the frequency domain, the gain and phase difference between response and transmitted signals will be calculated.

2.4. Compressive Sampling Theory

Traditionally, sampling theory has been largely based on the Nyquist/Shannon sampling theorem. Nyquist/Shannon dictates that to sample a signal while avoiding aliasing, the sampling frequency should be at least twice the highest frequency component in the signal. Aliasing is a phenomenon that occurs when a signal is sampled at a rate that is not sufficient to realize the changes in the signal. Aliasing can cause distortion and folding in the signal, resulting in irretrievable information. In my novel approach, compressive sampling can sample below Nyquist rate without loss of information. The approach aims to reduce the time needed to characterize the frequency response of a radar system or medium in comparison to the standard SFCW approach. While OFDM can generate multi-tone test signals, compressive sampling takes advantages of the spectrum sparsity of the impulse radar's pulse signal.

The theory of CS was proposed by Donoho, Candes and Tao in 2004, and a series of papers have been published since 2006 [8, 9, 10]. Compressive sampling (CS) theory focuses on the actual information that is contained in the signal [11]. Rather than using the signal's bandwidth as the metric to choose sampling rates, the information structure is used. Thus, CS paves the way to utilizing under sampling.

Let $\boldsymbol{x}$ be a discrete time pulse signal of length N. Applying an orthogonal transform matrix Ψ transforms $\boldsymbol{x}$ to a domain where the signal has sparse representation. A signal is said to have sparse representation if it can be reconstructed by a subset of the transform coefficients without significant loss of information. The transform $\boldsymbol{\Psi}$ enabling this property is called the sparsity transform. The transform can also be portrayed as follows [11]

$$\boldsymbol{X} = \sum_{\boldsymbol{p=0}}^{\boldsymbol{N-1}} \boldsymbol{x_p}\, \boldsymbol{\Psi_p}$$

$\boldsymbol{\Psi}$ can be based on the discrete Fourier transform, discrete cosine transform, discrete wavelet transform or any transform capable of converting a temporal signal into a few dominant coefficients in a different domain. For my research, I have chosen to use the Discrete Fourier Transform (DFT). The aforementioned equation can be rewritten as [11]:

$$\boldsymbol{X} = \boldsymbol{\Psi x}$$

where $\boldsymbol{X}$ is a $Nx1$ vector with K sparsity. Furthermore, the sparsity transform or sparsity matrix will possess a strong decorrelation property, i.e., it makes most of the coefficients $\boldsymbol{X}$ small [12]. Once the signal $\boldsymbol{x}$ is transformed into the $\boldsymbol{\Psi}$ domain, M number of coefficients are randomly selected and so the signal becomes compressed. Following CS theory, the measurement vector $\boldsymbol{y}$ of $\boldsymbol{X}$ can be expressed as [11]:

$$\boldsymbol{y_{Mx1}} = \boldsymbol{\Phi_{MxN}}\, \boldsymbol{x_{Nx1}} = \boldsymbol{\Phi_{MxN}} \boldsymbol{\Psi_{NxN}^{-1}} \boldsymbol{X_{Nx1}}$$

where $\boldsymbol{\Phi}$ is a MxN matrix called the measurement matrix and M ($K < M < N$) is the number of measurements [11]. In addition, CS theory stipulates that if $\boldsymbol{\Phi_{MxN}\Psi_{NxN}}$ have the restricted isometry property (RIP) [13], then it is possible to recover the signal $\boldsymbol{x}$ from the measurements $\boldsymbol{y}$ by solving the l_1-optimization problem as follows:

$$\boldsymbol{X} = \arg min||\boldsymbol{X}||_1 , \ \ s.t. \ \boldsymbol{y} = \boldsymbol{\Phi\Psi^{-1}X}$$

where $\boldsymbol{\Psi^{-1}}$ is the inverse of $\boldsymbol{\Psi}$.

To verify that RIP exists, it is imperative to have a high measure of incoherence between $\boldsymbol{\Phi_{MxN}}$ and $\boldsymbol{\Psi_{NxN}}$. Findings in compressive sensing indicate that a general random basis has a high degree of incoherence with any basis, including the identity basis [12]. Hence, a random matrix can be chosen to be the projection basis, $\boldsymbol{\Phi_{MxN}}$. The number of measurements M, given that we are using the Fourier domain, can be calculated by [9]:

$$M = \ O(K \log N)$$

However, it is important to note that the sparsity K of the signal is unknown and not user controlled but rather is inherent to the signal. Consequently, several simulations are run to test different M values and a value M is selected based on user constraints. The number of measurements, M, needs to be greater than K, and smaller than the full size of the signal, N, in order to achieve good reconstruction. As M is increased, the reconstruction recovers the compressed signal with fewer errors. If M gets too close to N or equals N, then the signal is no longer effectively compressed, or it is without compression, respectively.

CS enables the signal to be compressed down by retaining only the aforementioned K number of coefficients and preparing it for transmission. Conversely, the compressed signal can be reconstructed given the appropriate digital signal processing tools. Effectively, in the OFDM radar system design, the CS algorithm will determine what frequencies are necessary to be sent out and what frequencies are not, and in turn that reduces the overall operating time and power consumption. Transmitting a smaller number of frequencies using CS reduces the test signal power consumption and test signal complexity while maintaining the test coverage and performance levels.

2.5. OFDM/Compressive Sampling Simulation Methodology

For validation purposes, we carry out a ground penetrating radar functional test with a modified version of a Synthetic High Resolution Radar (HRR) profile derived from Mahafza [14]. By utilizing this channel model, we are introducing a frequency dependent phase and gain change to the system. The introduced frequency dependency represents the amplitude attenuation and phase change characteristics observed in physical implementations of a radar system. The functional test is for a channel comprised of air and a single scatterer. The setup is illustrated in Figure 2. For the reflected signal in the time domain, a single distinct pulse will be produced. The functional test is first carried out with the SFCW method for transmission and response analysis, and is then performed using the proposed OFDM-CS method for transmission and response analysis [5].

For test validation, simulations have been carried out in MATLAB, where SFCW and OFDM-CS signals are generated with the same test parameters. An N-tone signal of bandwidth B is used for both SFCW and OFDM-CS test simulations.

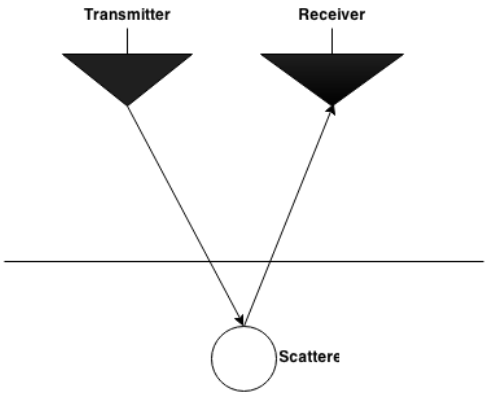

Figure 12 Model of the channel under test.

For SFCW testing method, a series of N tones is generated sequentially through the test configuration. In other words, N sinusoidal test stimulus signals are individually generated, applied, and responses measured in sequence. The DUT response under each stimulus signal is measured, and the respective magnitude and phase responses are extracted recorded in succession. After sweeping and testing all N frequency tones, all amplitude gain and phase response data are assembled in a matrix. Furthermore, by carrying out the IFFT calculation, the time domain impulse response can be obtained.

For OFDM-CS testing, the same N frequency points are applied as the SFCW test case. Using a single signal stream containing 1024 orthogonal frequency tones based on 1024 QPSK symbols. The signal has the same 100 MHz bandwidth as its SFCW counterpart. Hence, the frequency step size is 97.656 kHz resulting in a range resolution of

1.5 meters. This indicates that objects can be detected distinctly if they are spaced at 1.5 meters or more. Additionally, the transmitted signal's width is Figure 13(a) and figure 13(b) illustrates the magnitude of the generated OFDM baseband signal in time and frequency domain.

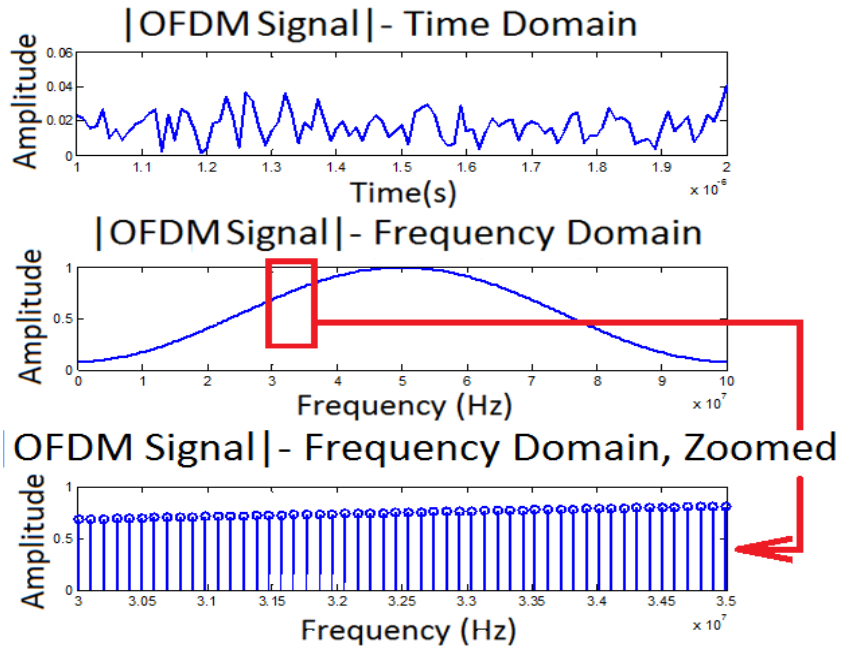

Figure 13 (a) Time domain representation of OFDM Transmit signal (b) Frequency domain representation of OFDM baseband signal (c) Section of the Frequency domain representation of OFDM baseband signal

Once the OFDM signal is generated in MATLAB, we pass it to the compressive algorithm, which will analyze the signal's sparsity. Once the sparsity is analyzed and a measurement matrix is computed, a subset of Fourier coefficients is selected for transmission. A compression factor of 1.7X less points (approximately 600 points instead of 1024 points) is used for the following discussion. Figure 14 (a) and 14 (b) illustrates the OFDM-CS transmit signal before it is sent through the test medium.

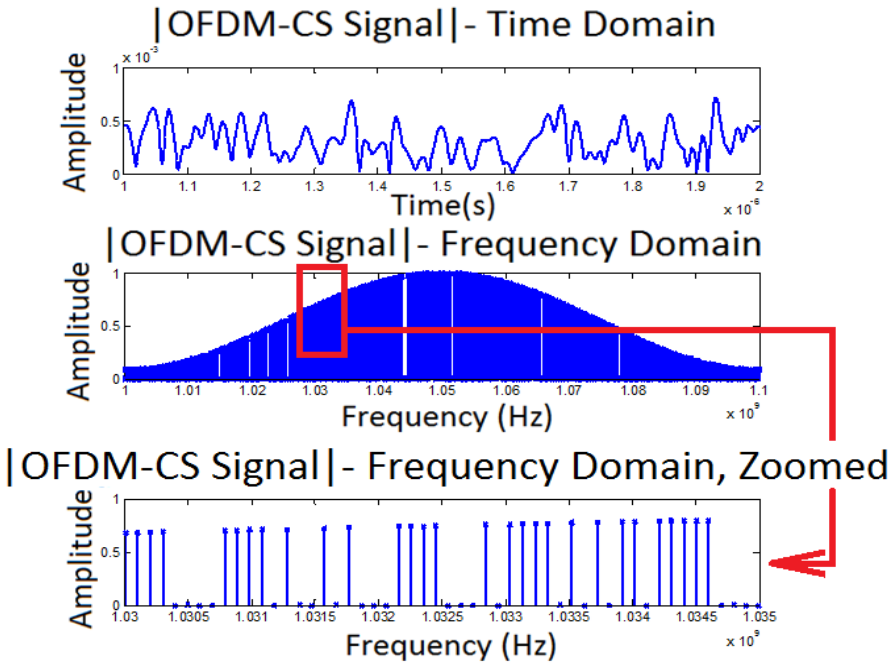

Figure 14 (a) Time domain representation of OFDM-CS Transmit signal (b) Frequency domain representation of OFDM-CS Transmit signal (c) Section of Frequency domain representation of OFDM-CS Transmit signal

The reflections are then discretized by sampling and are passed through the reconstruction algorithm along with the measurement matrix. An initial guess will start off the reconstruction process using an iterative l1-minimization solver. The reconstruction is passed through the FFT algorithm, where the response signal's amplitude and phase data are recorded for all encoded 1024 tones. The gain and phase differences are computed and recorded in a matrix that is used to illustrate the test channel's frequency response. In order to smooth out the data and to remove high frequency noise, we apply the two standard deviation rule and a moving average filter. In Figure 15 (b) and 16 (b), the amplitude and phase responses obtained from OFDM-CS method are plotted.

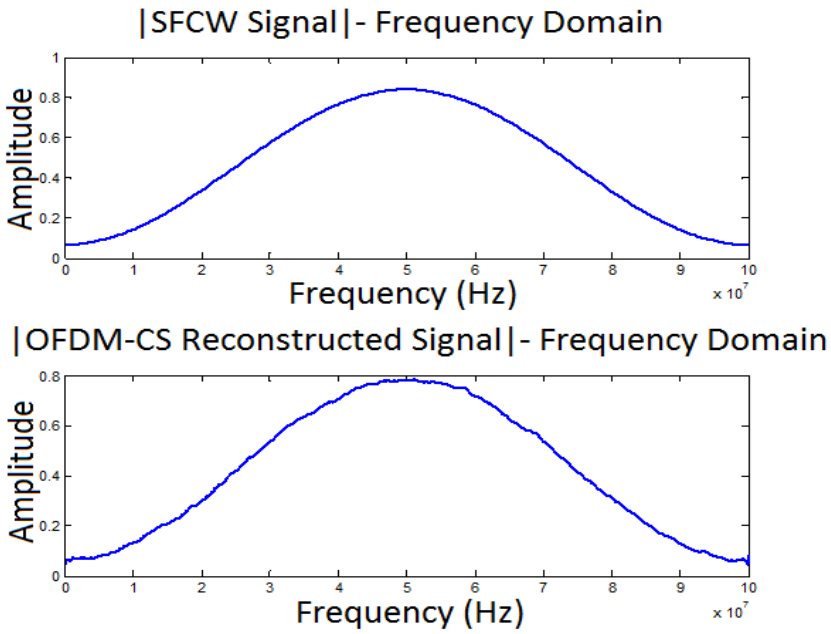

Figure 15 Amplitude responses using (a) SFCW and (b) OFDM-CS

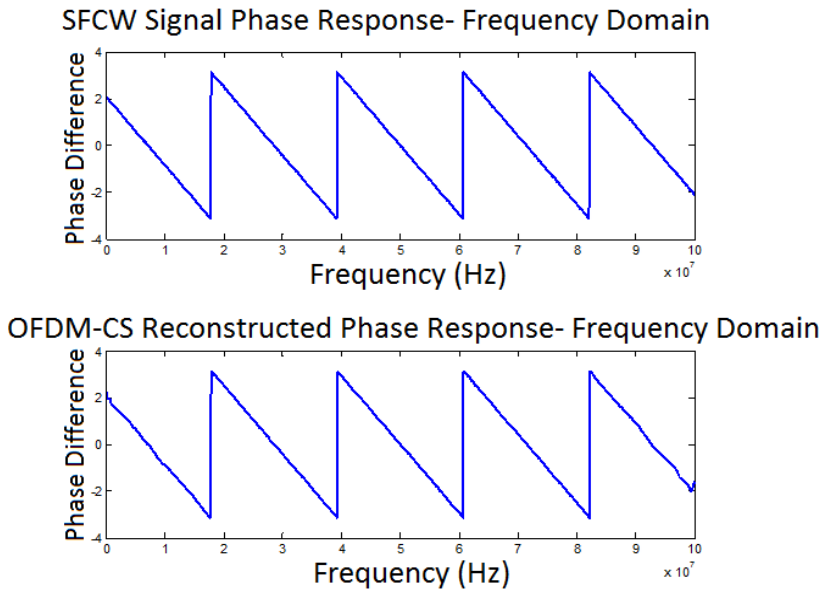

Figure 16 Phase responses using (a) SFCW and (b) OFDM-CS

By comparing SFCW and OFDM-CS test responses, it can be observed that Figure 15 and 16 show nearly identical gain and phase response from both testing methods. For further quantitatively comparison, Figure 17 illustrates a cross correlation between SFCW and OFDM-CS's gain responses. It is seen cross correlation peaks at 0.99, which indicates highly identical test responses employing OFDM-CS and SFCW testing methods.

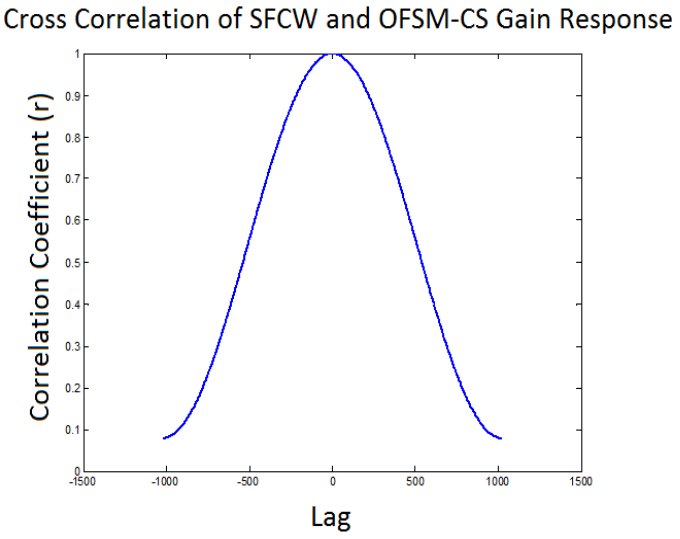

Figure 17 Cross-correlation of SFCW and OFDM-CS gain responses

For further validation of the success of the OFDM-CS approach, the time domain test response signals for both SFCW and OFDM-CS upon IFFT calculations are in Figure 18. Again, it shows nearly identical shapes and amplitudes for the time domain response signals. These results affirm that OFDM-CS accomplishes the benefits of increased test efficiency and spectrum coverage, while simultaneously maintaining the performance of SFCW test and decreasing the scanning time needed through reduction of required frequency tones by a factor of 1.7X less.

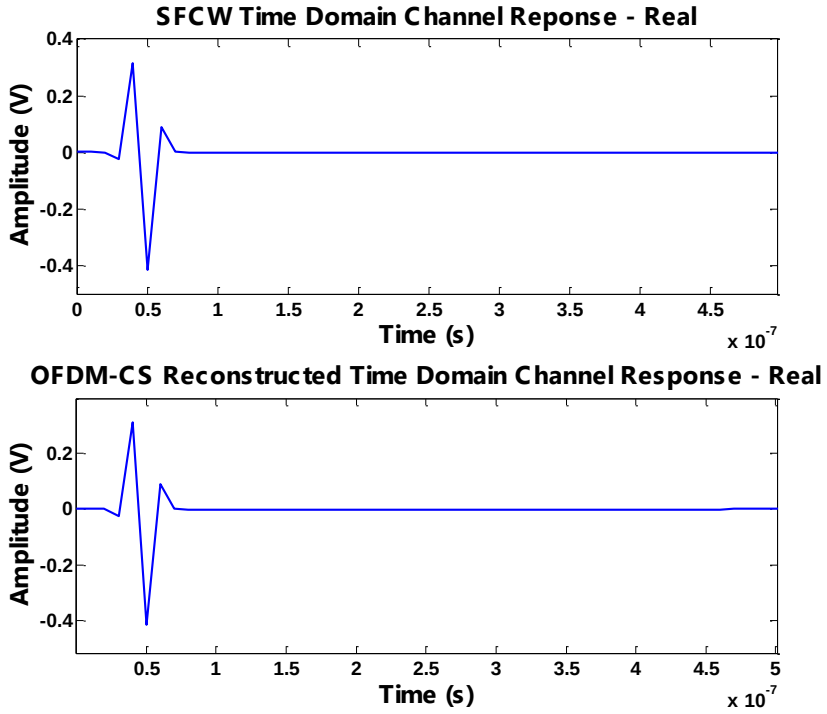

Figure 18 Time domain response using the (a) SFCW testing method (b) using the OFDM-CS method

In addition, a final quantitative metric, namely Signal-to-Error ratio (SER), is introduced to corroborate the results. SER is more sensitive metric in comparison to its correlation counterpart. SER of a simulated signal is calculates as follows:

$$SER = \frac{\sum_{a=1}^{1024} Y_a^2}{\sum_{a=1}^{1024} (Y_a - X_a)^2}$$

$$Y_a - Reconstructed\ Signal$$

$$X_A - Original\ Signal$$

The frequency spectrums for SFCW and OFDM-CS shown in Figure 5a and 5b are used to compute the SER. Given a compression of 1.7X less (600 points out of 1024), a SER value of 40 dB is computed which indicates a very small error in the reconstruction. In order to

choose a suitable M number of observations, the user needs to set constraints to define what level of correlation and SER is considered acceptable. These constraints will vary depending on the application and the compressibility of the signal. Given the aforementioned simulated signal, 10 different compression rates were applied and the metric results were recorded in Figure 19, 20, and Table 2. For example, if the constraints were to choose a compression rate resulting in an SER more than 30dB and a correlation more than 0.95 then M = 200 becomes a viable choice.

M Observations	**Compression**	**SER (dB)**	**Correlation**
100	10.24X	29.0	0.9994
200	5.12X	32.7	0.9997
300	3.41X	33.3	0.9998
400	2.56X	35.7	0.9999
500	2.04X	39.1	0.9999
600	1.70X	40.0	0.9999
700	1.46X	41.6	1
800	1.28X	47.1	1
900	1.14X	47.8	1
1024	1.00X	194	1

Table 2 SER and Correlation for difference compression rates

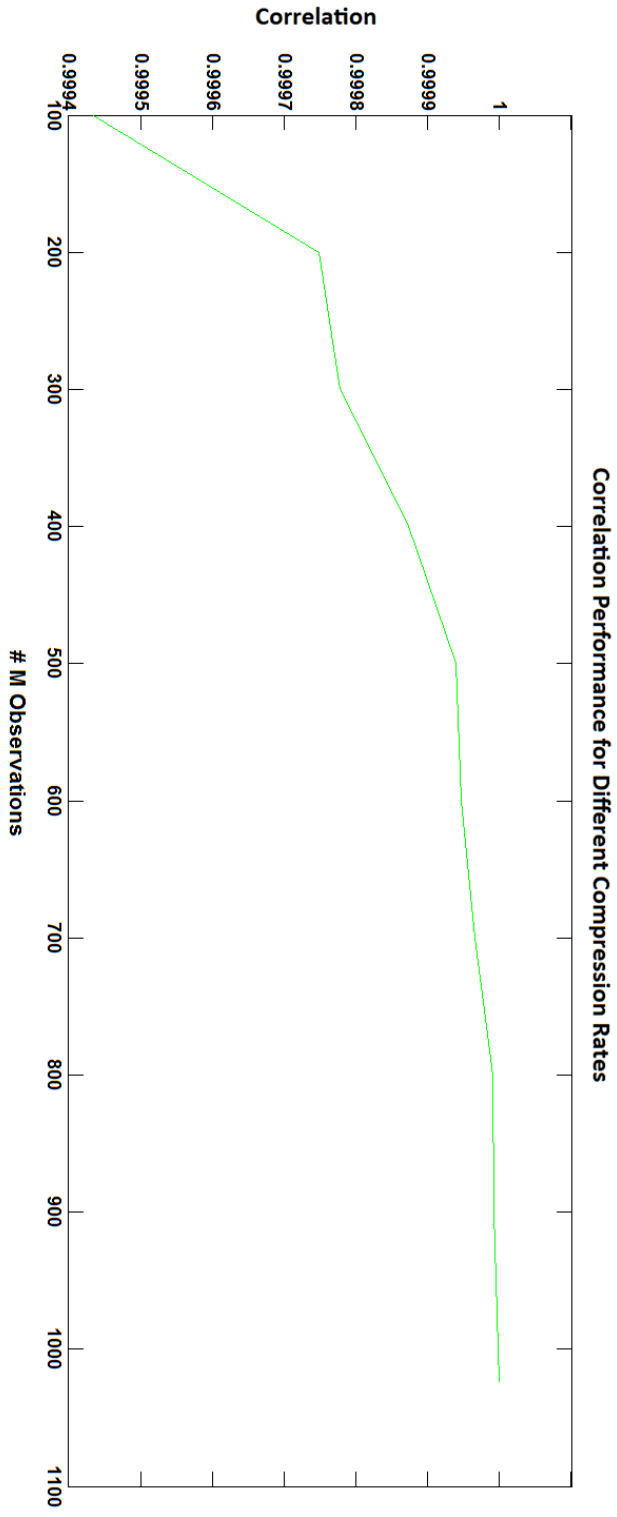

Figure 19 Correlation for difference compression rates

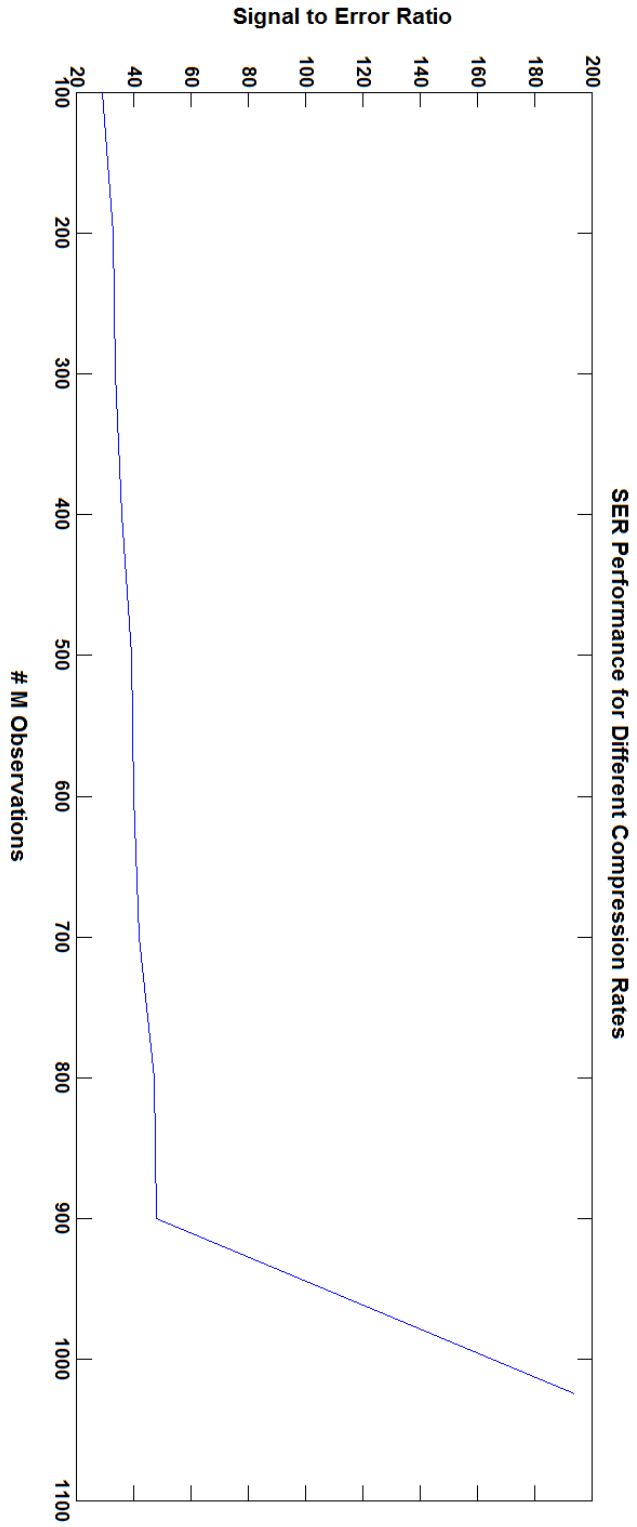

Figure 20 SER for difference compression rates

2.6. Hardware Design Theory and Methodology

An approach to verify the proposed test method can be implemented with inexpensive off the shelf hardware. Figure 21 illustrates a block diagram outlining the compressive sampled OFDM method's test bed being used.

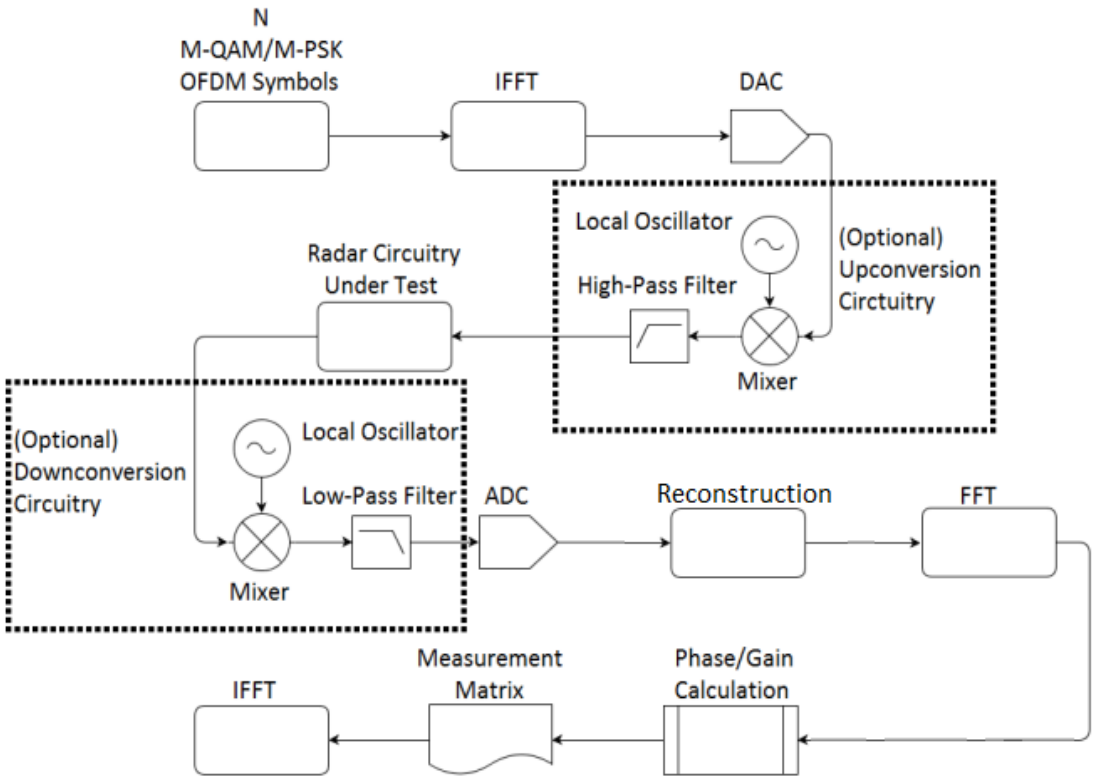

Figure 21 Block diagram of an OFDM Radar testing architecture.

The OFDM signal is generated using MATLAB, which is then exported to a memory file to be initialized into an FPGA. Through different modifications in the script, an array of arbitrary signals can be created. A DAC controlled by an FPGA allows the synthesis of the signal created in MATLAB. The ODFM signal is then modulated with a carrier signal, and transmitted through the DUT. Whilst the test signal is synthesized at

baseband, changing the carrier frequency enables the characterization over a large bandwidth. This is achieved through the use of a commercially off-the-shelf wideband PLL. Once received, the response is down converted back to baseband. Single-stage filtering allows the removal of higher frequency components created from the mixing process, as well as the removal of high frequency noise. At baseband, inexpensive ADC hardware can be used to sample the response signal. Responses must then be passed a reconstruction algorithm to recreate the full response over the bandwidth of the OFDM signal. The entire process is repeated multiple times with different carrier frequencies to test a wide operational bandwidth.

Functionally, the implementation of hardware will be similar to Langman's design, shown below in Figure 22.

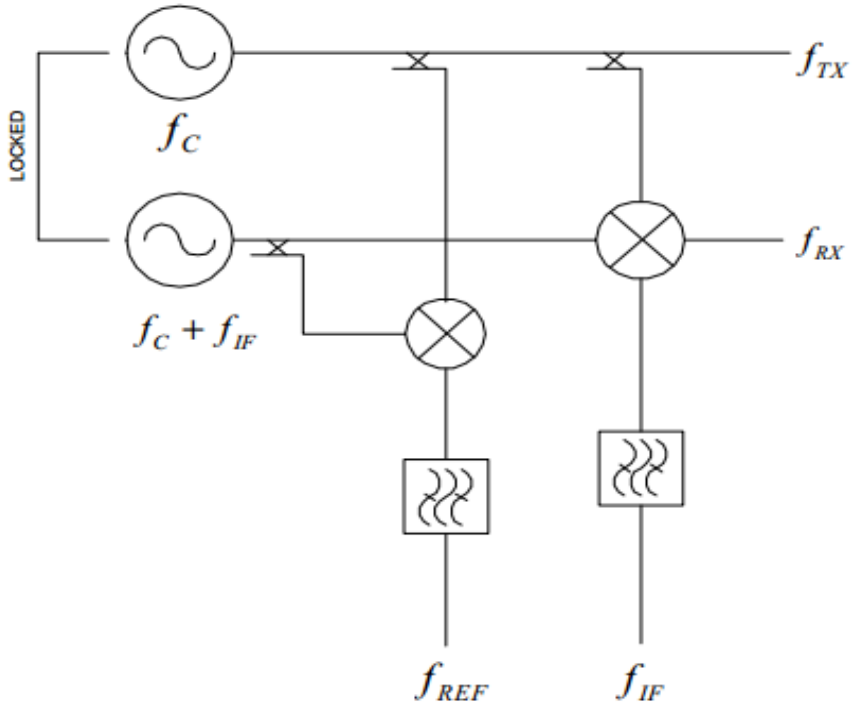

Figure 22 Langman's circuit diagram of heterodyne radar architecture.

A heterodyne architecture allows easier filtering of harmonics, and reduced subjectivity to temperature drift and flicker noise [11]. We can use this heterodyne architecture and implement the OFDM-CS test methodology with minimal changes

A device can be characterized with SFCW, OFDM, and compressive sampled OFDM using this one implementation of hardware. Different testing methods are employed by simply changing the contents of the memory file initialized to the FPGA, and thus the waveform that is transmitted. Equivalence of the improved testing methods can be shown using the hardware design described.

2.7. Conclusion

For radar systems implemented with ultra-wideband bandwidths, the time it takes to characterize the frequency response of the device-under-test increases considerably. We have proposed testing radar circuitry using the compressive sampled coupled OFDM method so as to leverage the test efficiency while maintaining comparable performance. Equivalence between CS-OFDM tests and SFCW test by characterizing the phase and amplitude responses is validated through test simulations. We plan to further this research by implementing the design on FPGA hardware for validations.

References

[1] Sylla, I. T., “Building an RF source for low cost testers using an ADPLL controlled by Texas Instruments digital signal processor DSP TMS320C5402,” IEEE International Test Conference, November 2003.

[2] Lu, A.K., Roberts, G..,"An oversampling-based analog multitone signal generator," Circuits and Systems II: Analog and Digital Signal Processing, IEEE Transactions 45, 391–394. 1998.

[3] Uemori, S., Yamaguchi, T., Ito, S., Tan, Y., Kobayashi, H., Takai, N., Niitsu, K., and Ishikawa, N., "ADC linearity test signal generation algorithm," IEEE Asia Pacific Conference on Circuits and Systems, December 2010.

[4] Watanabe, K., Asami, K., Furukawa, Y., Ueda, M., Watanabe, T., Purtell, M. "WCDMA testing with a baseband IF range AWG," IEEE International Test Conference. 2002..

[5] Metwally, M., L'Esperance, N., Xia, T., Slamani M. (2013, November). Continuous Wave Radar Circuitry Testing Using OFDM Technique. IEEE 32nd VLSI Test Symposium.

[6] Xia, T., Shetty, R., Platt, T., & Slamani, M. (2013). Low Cost Time Efficient Multi-tone Test Signal Generation Using OFDM Technique. Journal of Electronic Testing, 29(6), 893-901

[7] Xia, T. "Techniques to leverage test speed of wide band circuit/system-multitone sign generation and characterization," IEEE VLSI Test Symposium (VTS)'13 Elevator Talk.

[8] D. Donoho, "Compressed sensing," IEEE Trans. Inf. Theory, vol. 52, no. 4, pp. 1289–1306, Apr. 2006.

[9] E. Candes, J. Romberg, and T. Tao, “Robust uncertainty principles: Exact signal recovery from highly incomplete information,” IEEE Trans. Inf. Theory, vol. 52, no. 2, pp. 489–509, Feb. 2006.

[10] E. Candes and J. Romberg, “Sparsity and incoherence in compressive sampling,” Inv. Probl., vol. 23, no. 3, pp. 969–985, Jun. 2007.

[11] Ying, L., Zhang, Q., Hong, W., & YiRong, W. (2012). Waveform design and high-resolution imaging of cognitive radar based on compressive sensing. SCIENCE CHINA Information Sciences.

[12] Suksmono, A. B., Bharata, E., Lestari, A. A., Yarovoy, A. G., & Ligthart, L. P. (2010). *Compressive stepped-frequency continuous-wave ground-penetrating radar*. *Geoscience and Remote Sensing Letters, IEEE, 7(4)*, 665-669.

[13] Sarkas, I. (2010). Step Frequency Radar Using Compressed Sensing. *Department of Mathematics of the University of Toronto, Tech. Rep.*

[14] Mahafza, B.R. 2000. “Radar systems analysis and design using Matlab,” Chapman & Hall/CRC, Boca Raton.

CHAPTER 3: OFDM COUPLED COMPRESSIVE STEPPED-FREQUENCY CONTINUOUS WAVE RADAR TESTING ALGORITHM

3.1. Abstract

Non-destructive testing of man-made structures using ground penetrating radar (GPR) is very common today. Commercially, impulse radar is the favored radar architecture for structural testing purposes but it has its drawbacks. Stepped frequency continuous wave (SFCW) GPR is capable of overcoming these problems but suffers from low data acquisition speed. In this paper, we propose a new testing algorithm to increase data acquisition speed with low cost and low design overhead, by combining OFDM (Orthogonal Frequency Division Multiplexing) in conjunction with compressive sampling (CS) techniques. OFDM equips SFCW with the capability of sending multiple frequencies simultaneously, reducing scan time. Additionally, compressive sampling techniques reduce the total amount of frequencies required for characterizing the structure under test, further accelerating acquisition speed while lowering mean radiated power. To show equivalent performance between the GPR implementation methods, SFCW and OFDM-CS SFCW are both used to characterize a realistic bridge deck model.

3.2. Introduction

Ground Penetrating Radar (GPR) has been extensively used in the past two decades for a variety of applications, such as assessing transportation infrastructure. According to the U.S. Department of Transportation, over 40 percent of the bridges in the United States are classified as structurally deficient or functionally obsolete, with the

estimated cost of repairs running into billions of dollars [1]. Bridge deck deterioration is one of the most significant problems encountered with bridges' structural faults. Without being able to "see" the deterioration within the layers of the bridge deck, decisions on how to repair and manage the bridge lack certainty.

The objective is to improve methods of characterizing an environment, bridge deck condition in this case.

A variety of characterizing methods exist for deck condition assessment, such as chain drag, chloride content measurements, or resistivity methods. However these methods are labor intensive and require inconvenient lane closures. Furthermore, these methods are unable to adequately detect early stages of deterioration. In contrast, nondestructive techniques such as ground penetrating radar is non-contact and can test larger portions of the bridge deck at a relatively rapid speed. GPR has been mainly implemented using two different approaches.

The first approach is the Impulse Radar method. Typically, a pulse is transmitted through the medium being tested and the echoes (received signal) are collected and analyzed for information about the medium. The pulse is usually very narrow in time resulting in an extremely wide bandwidth frequency domain. The approach is realized using simple architecture. Given how narrow the pulse is in the time domain, scan times are short in duration. However, its drawbacks feature limited dynamic range and high cost of production. Dynamic range is defined as the ratio of the maximum signal power a system can tolerate without distortion of the signal, to the noise level of the system. The dynamic range problem stems from the signal being very wide in frequency, limiting filtering

capabilities that would help isolate the information from the noise floor. The expensive production costs are due to the very high sampling Analog to Digital Converters (ADC) and Digital to Analog Converters (DAC). These components are required to sample the very wideband signals while adhering to Nyquist sampling rate.

The second approach is Continuous Wave (CW) radar. CW does not transmit a pulse, but instead synthesizes the transmission of an impulse signal. An impulse can be decomposed into individual frequency components. CW systems transmit each of the frequency components of an impulse individually, and record the response. A common CW architecture is stepped frequency continuous wave (SFCW). SFCW radar systems work by sequentially transmitting individual frequency tones through the channel. The response signal is then received and sampled, and the phase and magnitude changes are calculated. After testing all of the frequencies in the operational bandwidth, an FFT algorithm can be used to transform the frequency characterization into a time domain impulse response. SFCW enjoys a high dynamic range, as filters can isolate each of the narrowband frequencies tones from the noise floor. In addition, a higher Signal to Noise ratio is achieved as more power can be concentrated per transmitted individual frequency tone. Furthermore, SFCW architecture does not require the expensive hardware that impulse systems use. SFCW does face one primary drawback; each frequency tone must be generated, transmitted, and received individually, resulting in longer SFCW operation than its impulse counterpart.

SFCW radar systems are often tested using a functional test, although this faces the same drawbacks outlined above. Improvements can be made to SFCW test methods to

reduce test time and leverage test efficiency. Some architectures will utilize phase locked loops (PLLs) to generate single frequency tones. To speed up test times, a common approach is to generate and test multiple frequency tones simultaneously. Many designs incorporate multiple PLL circuits to simultaneously generate frequencies. Designs utilizing one or more PLL circuits can still prove to be slow test methods, due to the time it takes for a PLL to 'lock' into a frequency. Rather than using one or more PLLs, some test circuits utilize Arbitrary Waveform Generators (AWG) [2], [3]. AWGs can be programmed to create signals containing various frequencies and phases. An AWG's customizable signal is often used for production tests and characterization. However, a traditional AWG requires considerable amount of memory for data pattern storage, and can cost over $10,000. Due to the expense and cumbersome nature of AWGs, often they are infeasible for testing. An alternative method of signal generation can be implemented using an FPGA and a high speed DAC, as proposed in an earlier publication [4]. The testing method proposed allows the arbitrary creation of signals, permitting Orthogonal Frequency Division Multiplexing (OFDM) and the application of compressive sensing (CS) theory to characterize the condition of bridge decks using B-scans.

3.3. Compressive Sampling Theory

Conventionally, sampling rates are selected based on the Nyquist/Shannon sampling theorem. Nyquist/Shannon dictates that to avoid corruption, the sampling frequency has a lower bound at twice the highest frequency component in the signal. This frequency is known as the Nyquist Rate. By sampling below the Nyquist Rate,

unintentional aliasing can occur, where information is folded onto itself. Compressive sensing techniques can allow sampling below the Nyquist rate, without the loss of information. To do so, compressive sampling takes advantage of the sparsity of a signal, in this case particularly, the impulse signal's spectrum in frequency domain.

The theory of CS was proposed by Donoho, Candes and Tao in 2004, and a series of papers have been published since 2006 [5,6,7]. Compressive sampling (CS) theory is information driven, focusing on the actual signal to be used in the test [8]. Instead of using the signal bandwidth to derive sampling rates, the information structure is used. Thus, CS enables the use of under sampling. Practically, a CS algorithm will determine what frequencies are necessary to be transmitted, and what frequencies can be omitted without significant loss of information.

Let $\boldsymbol{x}$ be a discrete-time signal of length N. This signal is said to be K sparse if it can be represented in some domain by K coefficients, where $K < N$. This representation can be achieved using an orthogonal transform matrix $\boldsymbol{\Psi}$. This matrix can be based on any injective transform that can convert a temporal signal into a few dominant coefficients in a different domain. In this paper, Discrete Fourier Transform is used for $\boldsymbol{\Psi_p}$, where the signal has K sparse representation with $K < N$. This can also be portrayed as follows [8]

$$\boldsymbol{X} = \sum_{\boldsymbol{p=0}}^{\boldsymbol{N-1}} \boldsymbol{x_p}\, \boldsymbol{\Psi_p}$$

The aforementioned equation can be rewritten as:

$$\boldsymbol{X} = \boldsymbol{\Psi x}$$

where $\boldsymbol{X}$ is a $Nx1$ vector with K sparsity and $\boldsymbol{\Psi}$ is called the sparsity transform. The sparsity transform or sparsity matrix will possess a strong decorrelation property, i.e., it makes most of the frequency coefficients of $\boldsymbol{X}$ small [9]. Once the signal $\boldsymbol{x}$ is transformed into the new domain, M number of coefficients are randomly selected and so the signal becomes compressed. Following CS theory, the measurement vector $\boldsymbol{y}$ can be expressed as:

$$\boldsymbol{y_{Mx1}} = \boldsymbol{\Phi_{MxN}\Psi^{-1}_{NxN}X_{Nx1}}$$

where $\boldsymbol{\Phi}$ is the MxN measurement matrix and M $(K < M < N)$ is the number of measurements [8]. In addition, CS theory stipulates that if $\boldsymbol{\Phi_{MxN}\Psi_{NxK}}$ have the restricted isometry property (RIP) [10], then it is possible to recover the signal $\boldsymbol{x}$ from the compressed measurement vector $\boldsymbol{y}$ by solving the l_1-optimization problem as follows:

$$\boldsymbol{X} = \arg min||\boldsymbol{X}||_1 , \ s.t. \ \boldsymbol{y} = \boldsymbol{\Phi\Psi^{-1}X}$$

where $\boldsymbol{\Psi^{-1}}$ is the inverse of $\boldsymbol{\Psi}$.

Based on the simulation and validation results, it has been observed that the compressive algorithm in my approach will function effectively as long as two conditions are met at all time for number of measurements M. The conditions are:

1. M exceeds the physical sparsity K of medium being characterized

2. $M < N$ where N is the total length of the signal

According to Candes, if K is known then M can be calculated, given that we are using the Fourier domain, as follows [6]:

$$M = O(K \log N)$$

However, the sparsity K of the environment under test, is unknown. To tackle this, several simulations are executed with varying values of M. The algorithm is automated to select a suitable point M based on user specified constraints. The acquisition of M is explained later in the simulation methodology section. Transmitting fewer frequencies reduces the test signal power and complexity while maintaining the test bandwidth and performance levels.

3.4. OFDM Theory

OFDM allows the generation of a multiple orthogonal frequency tones to create a single signal, without loss of information contained in each individual tone. Transmitting frequencies that are orthogonal to one another mitigates the interference between frequency tones. Orthogonality between tones requires the sub-bands to be placed at $Fa = \frac{k}{T_S}$.

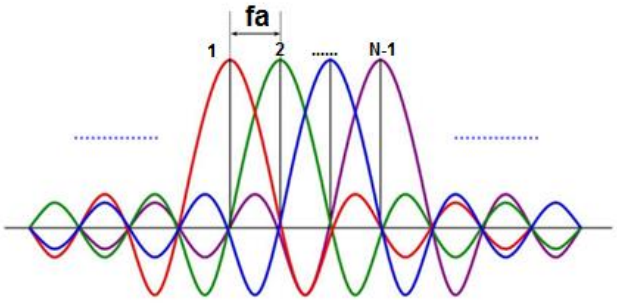

Figure 23 Frequency spectrum of N-tone OFDM signal

where Ts is the OFDM symbol period, and k is any integer.

For OFDM symbol generation, a square wave spectrum with constant amplitude and phase can be employed for multi-tone signal generation. However, there is a significant drawback, in that the IFFT of a rectangular wave spectrum produces a sinc function in time domain, wherein except the data points on the main lobe, all others have small values. Due to noise, any information not contained in the main lobe could be lost or corrupted due to a low signal to noise ratio. To address this, my implementation utilizes the 4-QAM (QPSK) scheme, where symbol amplitudes are randomly assigned to ±1±1j for the real and imaginary components [11, 12]. Upon IFFT, the time domain signals have relatively higher amplitudes and higher signal to noise ratio, which can alleviate the noise impact and improve test accuracy. SFCW's spectrum is user defined and typically truncated, taking on a rectangular shape. In an impulse radar, the transmitted signal's bandwidth is trimmed and shaped by the antenna response. By definition, the waveform's bandwidth is defined as the width of the signal's spectrum at 3dBs below the peak response. Figure 24 illustrates a comparison between the resolution and side lobe level for an impulse and SFCW waveform, following the aforementioned definition.

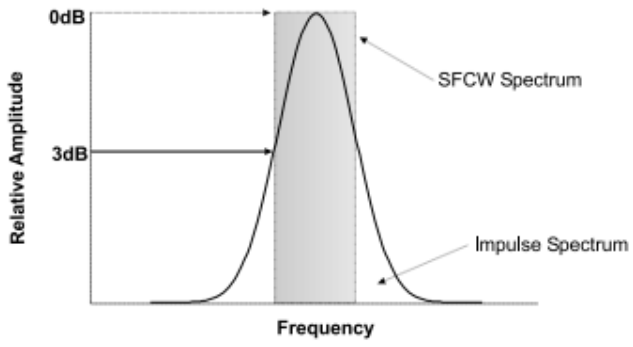

Figure 24 Comparison between SFCW spectrum and Gaussian shaped impulse spectrum [13]

Gaussian shaped impulse and SFCW spectra operating within the same 3dB bandwidth is seen in the above Figure. The resulting impulse response from using both spectra is shown in Figure 25. Obviously, the SFCW response is quite bleak in contrast with its impulse radar response.

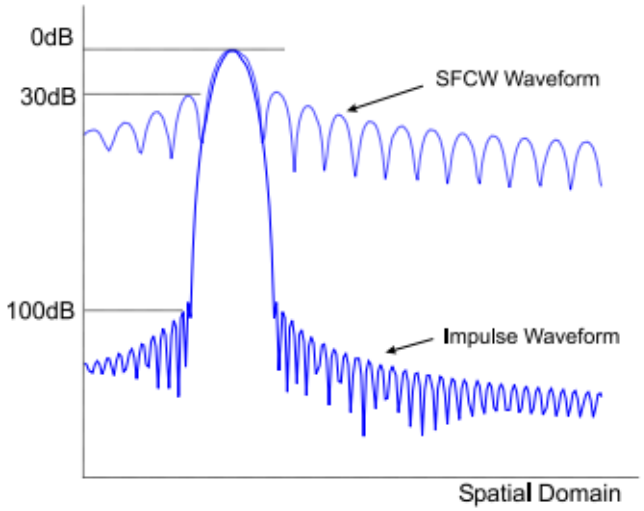

Figure 25 Resulting responses for SFCW and Impulse radar spectra [13]

The side lobes of the SFCW's response can be reduced by weighting the spectrum. If the SFCW spectra is weighted with a window that has the same envelope as the envelope of the spectrum of the impulse radar waveform and we ensure that both spectra cover the same carrier frequency span, then both waveforms will have the same impulse response [13]. The weighted SFCW response will be the identical as shown in Figure 24, except the synthetic range response is now generated by applying a window. This window of choice is applied to the frequency domain data, ensuring the 3dB bandwidth points are identical to the impulse radar waveform [13]. Several windows were experimented with including Gaussian, Kaiser, Chebyshev, Hamming, and Hanning. Given my simulation needs,

Hamming was the optimal choice to obtain a practical time domain signal for transmission. Following a series of extensive simulations, QPSK random phase assignment was deemed not suitable for the transmitted signal. Its disqualification quells from its poor compressibility. There was no suitable domain found where the signal, given QPSK random phase, could be represented with a few dominant coefficients. Therefore, the phase was assigned using different phase shift keying constellations, namely Binary Phase Shift Keying (BPSK) and 8-PSK with gray coding. The compressibility of the transmitted signal did not improve using either scenario. The solution was to use linearly increasing phase. Given the full uncompressed signal, assigning linearly increasing phase would result in an impulse in the time domain. Figure 26 demonstrates the aforesaid impulse.

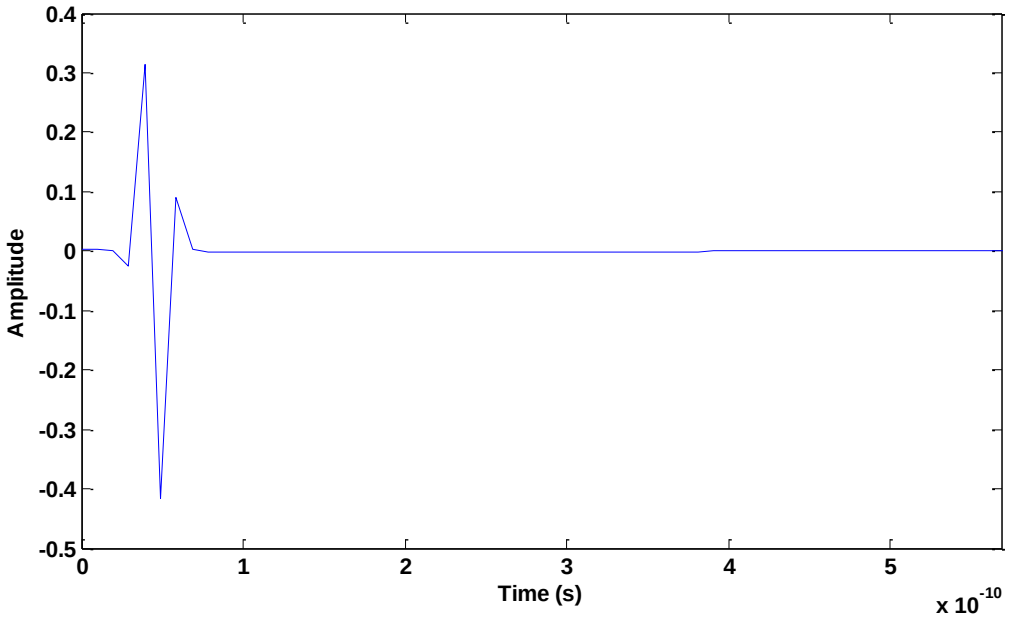

Figure 26 Time domain representation of OFDM with uncompressed linear phase

However, since we are compressing the signal, only a few frequencies are being utilized and consequently, only a few phase points are assigned to the transmit signal. When the compressed signal is transformed back to the time domain, a practical OFDM-CS signal is realized as illustrated in Figure 27.

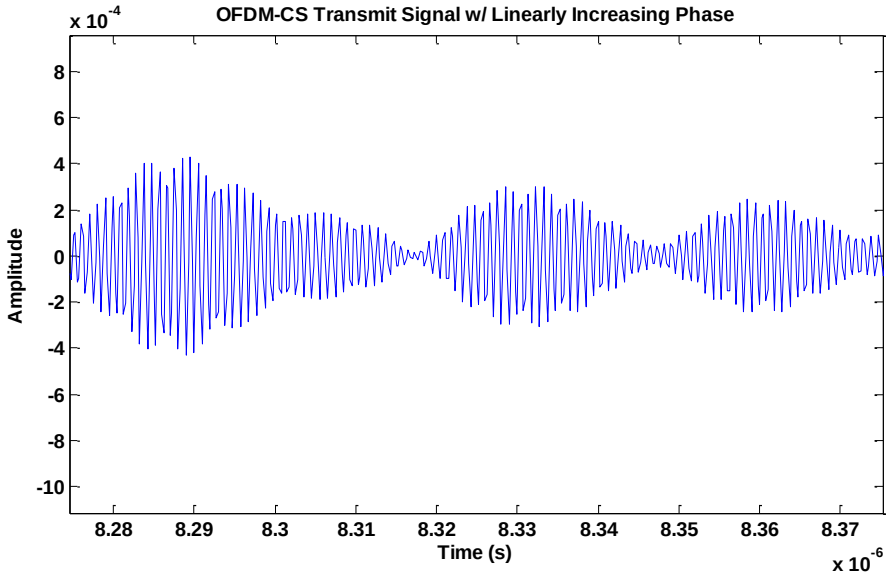

Figure 27 Time domain representation of OFDM with compressed linear phase

The generated OFDM signal can be up-converted if necessary, and transmitted through the medium or DUT for characterization. Once the signal response is received, it must be sampled by ADC hardware. If the signal was upconverted, it may be necessary to down convert the signal to baseband before sampling. The sampled signal is then passed through an FFT algorithm to return signal to the frequency domain. Once in the frequency domain, the gain and phase difference between response and transmitted signals will be calculated.

3.5. Simulation Methodology

3.4.1. Finite Difference Time Domain Channel Generation

For validation purposes, we carry out a ground penetrating radar functional test with a custom channel based on the Finite Difference Time Domain (FDTD) technique. FDTD is a numerical analysis method employed in modeling computational electrodynamics, specifically finding approximate solutions to Maxwell's equations. Computed in time domain, FDTD solutions cover a wide frequency range and treat nonlinear material properties in a realistic natural way. FDTD is a grid-based differential numerical modeling method that discretizes Maxwell's equations using central-difference approximations to the space and time partial derivatives. In deriving these equations [14], one of two sets of vectors is chosen:

1. Transverse Electric (TE) mode, comprising of: $E_x, E_y \; and \; H_z$
2. Transverse Magnetic (TM) mode, comprising of: $E_z, H_x \; and \; H_y$

Take the TM mode set for example, writing the governing equations out:

$$\varepsilon \frac{\delta E}{\delta t} = \nabla \times H - J$$

$$\frac{\delta H}{\delta t} = -\frac{1}{\mu_0} \nabla \times E$$

Where E and H are the electric and magnetic fields respectively. The conductive current density is:

$$J = \sigma E$$

$$\frac{\delta}{\delta z} = 0 \quad and \quad E_X = E_Y = H_Z = 0$$

Establishing the above listed conditions will enable us to obtain the non-zero components of $\frac{\delta E}{\delta t}$ and $\frac{\delta H}{\delta t}$.

$$\varepsilon \frac{\delta E}{\delta t} = (\frac{\delta H_y}{\delta x} - \frac{\delta H_x}{\delta y}) - \sigma E_z$$

$$\frac{\delta H_x}{\delta t} = -\frac{1}{\mu_0}\frac{\delta E_z}{\delta y}$$

$$\frac{\delta H_y}{\delta t} = -\frac{1}{\mu_0}\frac{\delta E_z}{\delta x}$$

The resulting finite-difference equations are solved sequentially; with every time instant, the electric field vector components are resolved in a given volume of space, or Yee cell [15] as seen in Figure 28.

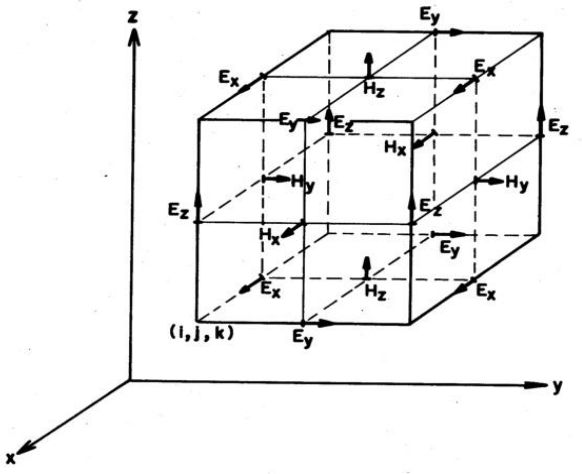

Figure 28 A Yee cell's illustration of how the different forces act [15]

The magnetic field vector components are resolved in the next instant of time. This process is reiterated until the entire computational grid is computed or certain conditions are met first. Due to FDTD's grid size restriction, the electromagnetic field cannot change over one

increment in the space gird, or Yee cell. As a result, to obtain meaningful results, it is necessary for the linear dimensions of the gird to be a fraction of the wavelength. This requirement places a restriction upon the time step (Δt) for the chosen gird dimensions. If the permittivity and permeability are constant, this restriction, known as the stability criterion, is articulated as:

$$c_{max} \cdot \Delta t \leq \sqrt{\left(\frac{1}{(\Delta x)^2} - \frac{1}{(\Delta y)^2}\right)}$$

Where c_{max} is the maximum velocity through a given medium defined as:

$$c_{max} = \sqrt{\frac{c}{\varepsilon_r}}$$

Where c is the speed of light in vacuum and ε_r is the permittivity of the medium.

In order to build the bridge deck model, a computational domain is first established. The domain is simply the physical region over which the simulation is applied. The electric and magnetic fields are determined at every grid point in space within the specified domain. Each grid point has to have a material attribute specified. The attributes are usually either free-space (air), dielectric or metal. Practically, any material can be specified through user input of the permittivity ε, conductivity σ and permeability μ values. Therefore, the FDTD based channel serves as a very robust and realistic model for the bridge deck, as it is flexible with how many objects/layers can be added and their material natures. For my validation purposes, we created a bridge deck that contains a layer of asphalt covering a concrete slab with an embedded metal rebar in its center as shown below in Figure 29.

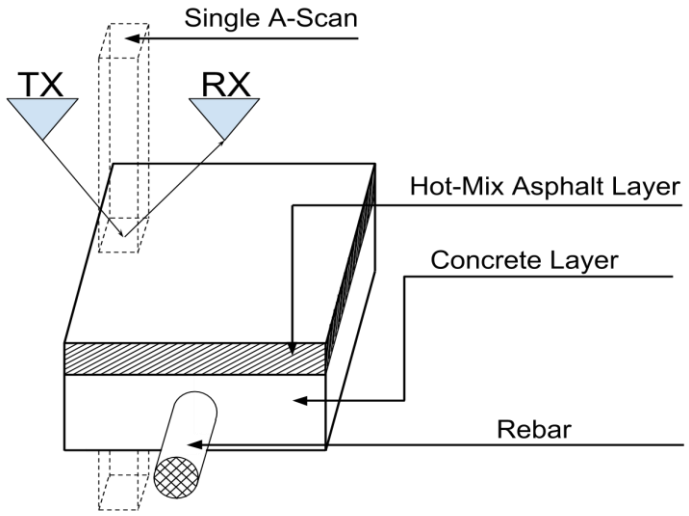

Figure 29 Mock-up of the channel created by FDTD

3.4.2. A-scan Generation

For test validation, simulations have been carried out in MATLAB where SFCW and OFDM-CS signals are generated with the same test parameters. A signal of bandwidth B is used for both SFCW and OFDM-CS test simulations. For SFCW testing method, a series of D tones is generated sequentially through the test configuration. In other words, D sinusoidal test stimulus signals are generated one by one in sequence. The FDTD channel response under each stimulus signal is measured individually, and the respective magnitude and phase responses are extracted recorded in succession. After sweeping and testing all D frequency tones, all amplitude gain and phase response data are assembled in a matrix. Furthermore, by carrying out the IFFT calculation, the time domain impulse response can be obtained. For OFDM-CS testing, the same D frequency points are applied similar to the SFCW case.

A single signal stream containing 1024 orthogonal frequency tones, based on 1024 QPSK symbols, is created. The signal's bandwidth is selected to be 800 MHz. With 1024 frequency steps spanning 800 MHz, the frequency step size is 781.25 kHz. These signal specifications provide a range resolution of 0.1875 meters and a maximum unambiguous range of 192 meters. Figure 30(a) and figure 30(b) illustrates the magnitude of the generated OFDM baseband signal in time and frequency domain.

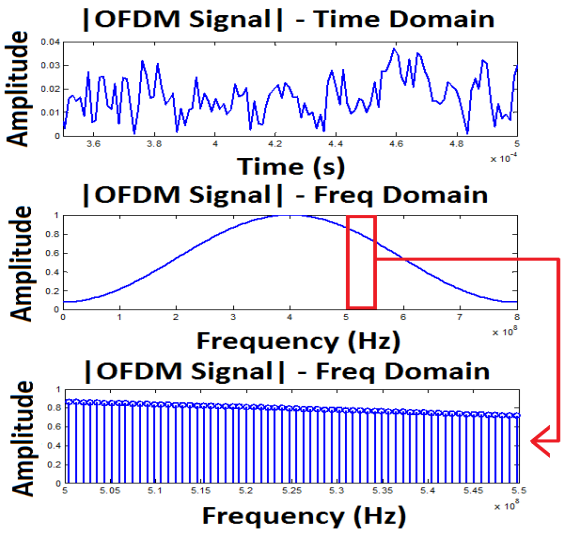

Figure 30 (a) Time domain representation of OFDM baseband signal (b) Frequency domain representation of OFDM baseband signal

Once the OFDM signal is generated in MATLAB, the algorithm selects M number of frequency tones for transmission. To determine a suitable number of observations M, a priori information needs to be provided in the form of an uncompressed frequency response. The calibration is done by transmitting the uncompressed OFDM signal through the channel under test. The gain and phase difference is extracted from the received OFDM

signal and used to establish the frequency response of the simulated channel. The frequency response, serving as a reference, is analyzed by the compressive algorithm to obtain M. The algorithm is set up to randomly pick a subset of frequency tones, M, and attempt to reconstruct the entire response. The error is then calculated between the reconstruction and the reference response. This error serves as a metric to determine what is considered an acceptable value for M. Given a user specified minimum error, a custom binary search is implemented to locate a suitable set of M frequencies. With the set of observations selected, the compressive algorithm applies the parameters to the OFDM signal, and generates an OFDM-CS signal. The OFDM-CS signal is then prepared for transmission into the channel under test, as portrayed in Figure 31. Additionally, this OFDM-CS signal is used for all subsequent A-scans. For the current channel model, M was determined to be at M = 500 frequencies given a minimum SER of 25 dB.

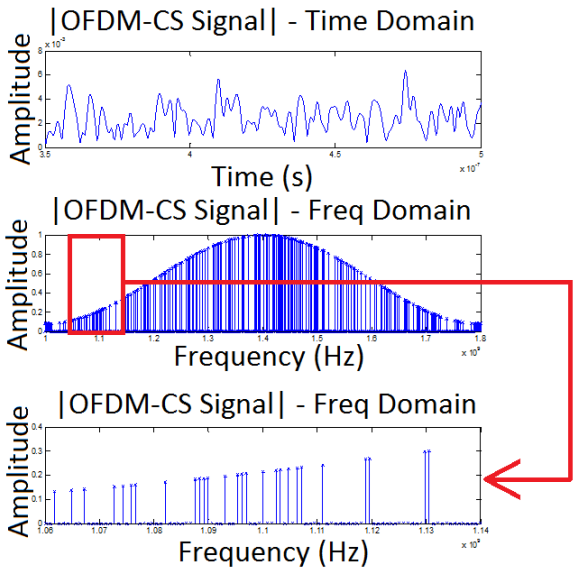

Figure 31 (a) Time domain representation of OFDM-CS transmit signal (b) Frequency domain representation of OFDM-CS signal

The reflections are then discretized by sampling and are passed through the reconstruction algorithm along with the measurement matrix and an initial guess that will provide a seed for the reconstruction l1-minimization based algorithm. The reconstruction is passed through the FFT algorithm where the response signal's amplitude and phase data are recorded for all encoded 1024 tones. The gain and phase difference are computed and recorded in a matrix that is used to illustrate the test channel's frequency channel. In order to smooth out the data and to remove high frequency noise, we apply the two standard deviation rule and a moving average filter. For performance comparison between the traditional SFCW and proposed OFDM-CS approaches, three metrics are employed:

1. Visual Comparison
2. Cross-Correlation
3. Signal-to-Error ratio (SER).

The first metric is self-explanatory and is shown below in Figure 32. It can be observed that visually, they are almost identical.

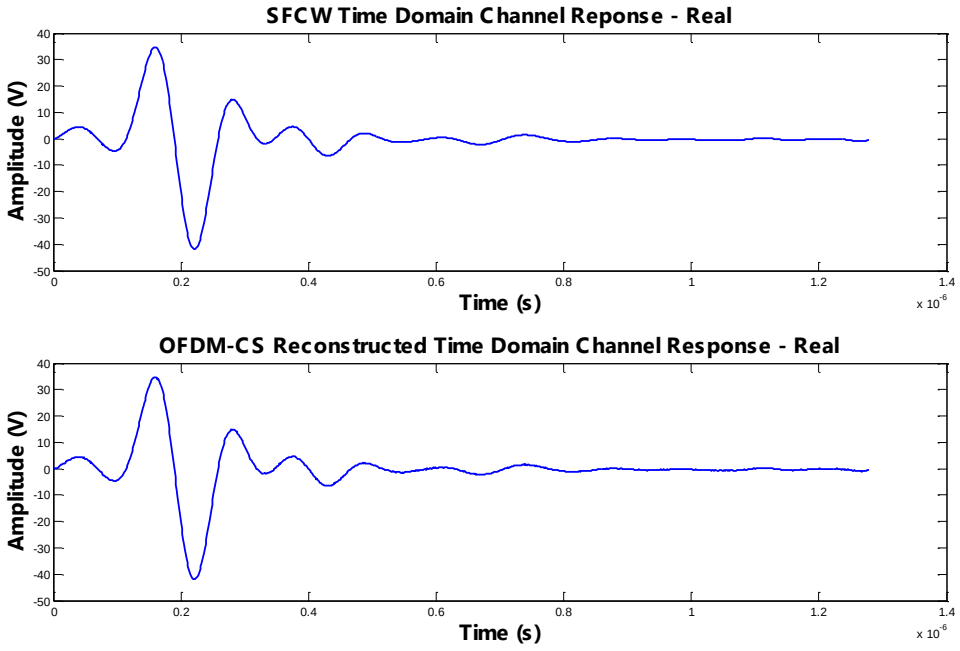

Figure 32 SFCW vs OFDM-CS channel response in time domain

While the first metric is qualitative, the rest are unbiased quantitative measures of performance. Cross-correlation measures the similarity between both the results of both approaches in the form of a value between 0 and 1. A value of 0 indicates absolutely no correlation or similarities between the two approaches while a value of 1 indicates perfect correlation. The equation below illustrates how the cross-correlation is computed:

$$\rho = \frac{cov(x, y)}{\sigma_x \sigma_y}$$

where cov( ) is the covariance, σ_x and σ_y are the standard deviations of SFCW data and OFDM-CS data respectively. It is seen that the cross correlation peaks at 0.9986, which indicates highly similar test responses employing OFDM-CS and SFCW testing methods.

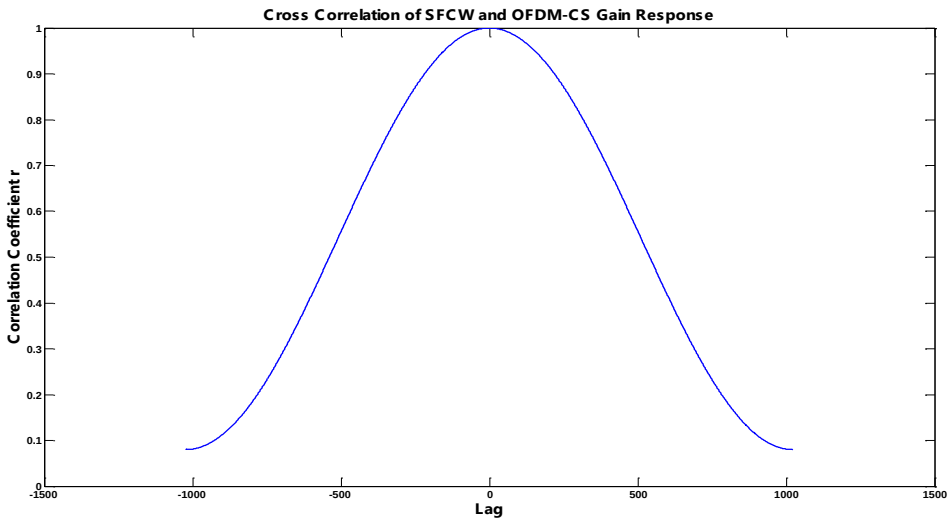

Figure 33 Cross correlation of SFCW and OFDM-CS Gain response

The SER measures how identical the results from the two approaches are. The following equation illustrates how the ratio is calculated:

$$SER = 10\log_{10}\left[\frac{\sum_{i=1}^{1024} X_i^2}{\sum_{i=1}^{1024}(X_i - Y_i)^2}\right]$$

where X_i : the i^{th} frequency tone response extracted with OFDM-CS and Y_i : the i^{th} frequency tone response extracted with SFCW. The SER for the current channel model with M = 500 was estimated at 25.3 dB. The A-scan generation process was repeated to cover different compression rate scenarios and analyze how the compressive algorithm responds. The algorithm's response was recorded using the correlation and SER metrics. Figure 34 and Figure 35 display the correlation and SER results for compression rates ranging from 1.02X to 10.2X. The results are further tabulated in Table 3.

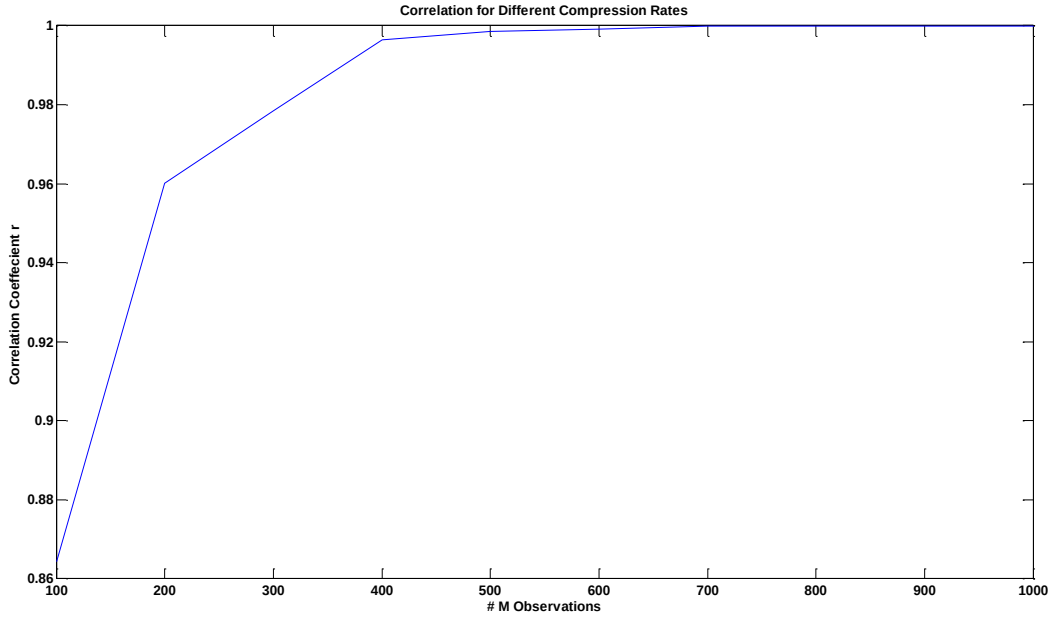

Figure 34 Cross correlation for different compression scenarios

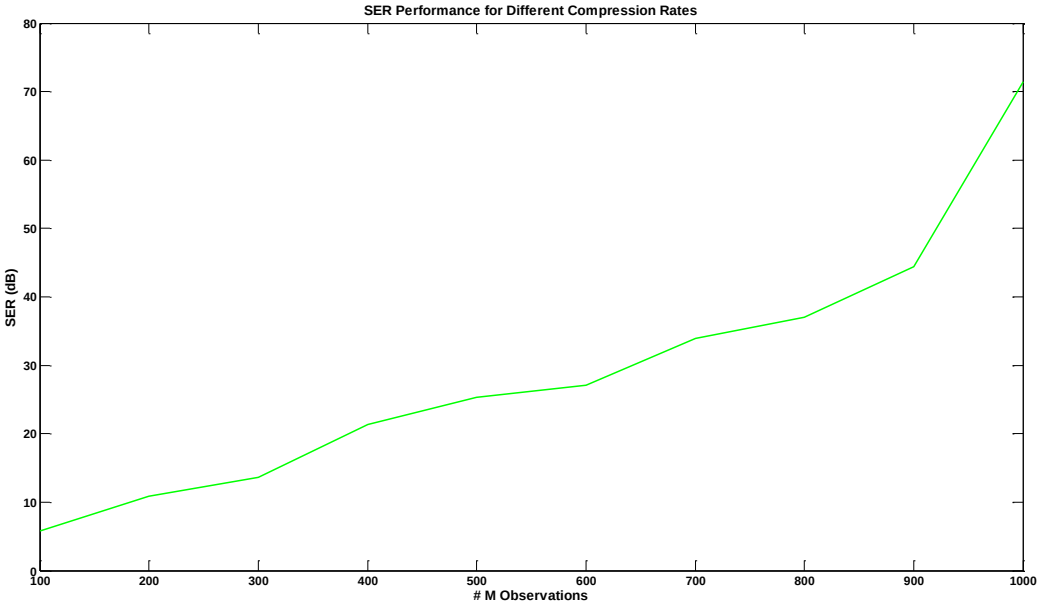

Figure 35 Signal-to-error ratio for different compression scenarios

M Observations	Compression Rate	SER (dB)	Correlation
1000	1.02X	71.4	1.0000
900	1.14X	44.4	1.0000
800	1.28X	37.1	0.9999
700	1.46X	33.9	0.9998
600	1.71X	27.0	0.9991
500	2.05X	25.3	0.9986
400	2.56X	21.3	0.9965
300	3.41X	13.6	0.9785
200	5.12X	10.8	0.9601
100	10.2X	5.8	0.8643

Table 3 Summary of metrics for different compression ratios - A-scan

3.4.3. B-scan Generation – Single Metal Rebar

With the A-scan calibration completed, the selected M number of observations is applied to a full scan of the entire channel. The selection of the M is user defined by specifying the minimum SER required for the transmit signal. The transmitter/receiver location is changed with every A-scan generated as to simulate the GPR physically moving over the bridge deck illustrated in Figure 36.

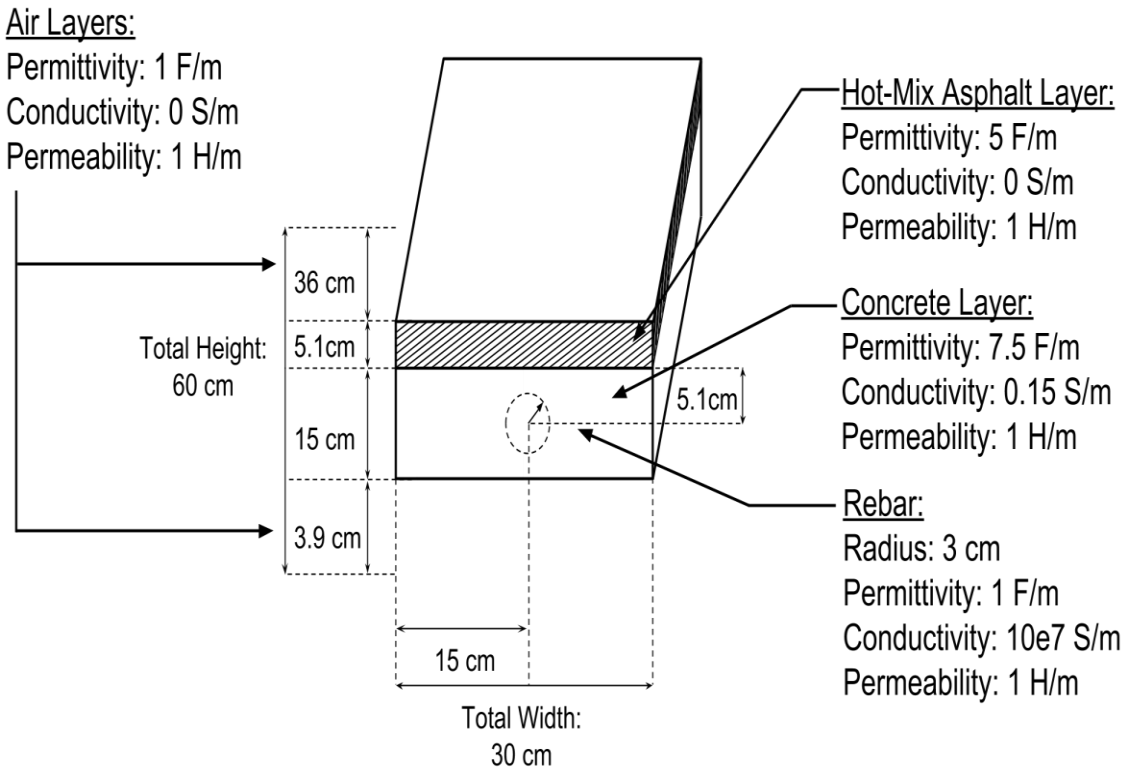

Figure 36 Detailed schematic describing channel parameters

Each A-scan is saved in a matrix that is used at the end to form a 2D image giving a cross-sectional view, namely, a B-scan as shown below in Figure 37. The parabola is a signature in industrial GPR systems indicating the presence of a metal rebar within the bridge deck section being scanned.

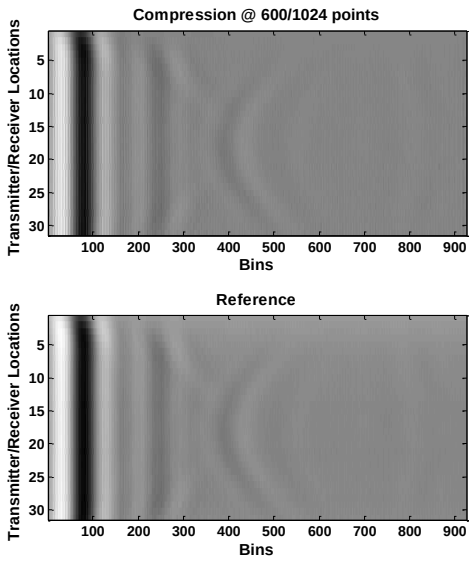

Figure 37 Reconstructed B-scan from 600 points compared with reference B-scan

While a visual examination of the above figure can indicate the high similarity between the proposed OFDM-CS methodology and the traditional SFCW methodology, a quantitative metric is certainly less subjective and less biased. A 2D correlation coefficient is computed to measure the similarity between the reconstructed under sampled B-scan and the reference B-scan as follows:

$$r = \frac{\sum_m \sum_n (A_{mn} - \bar{A})(B_{mn} - \bar{B})}{\sqrt{\left(\sum_m \sum_n (A_{mn} - \bar{A})^2\right)\left(\sum_m \sum_n (B_{mn} - \bar{B})^2\right)}}$$

where $\bar{A}$ and $\bar{B}$ are the matrix averages of A and B respectively

And the correlation coefficient was computed in the above-mentioned B-scan to be 0.9516. In addition, the SER was computed for the B-scan to be Furthermore, B-scans

were generated for the different compression rate scenarios and are illustrated in Figures .The B-scans were analyzed quantitatively respective SER and correlation values were recorded in Table 4. The results are illustrated in Figure 38 and Figure 39.

M Observations	Compression Rate	SER (dB)	Correlation
1000	1.02X	21.88	0.9516
900	1.14X	21.85	0.9516
800	1.28X	21.83	0.9516
700	1.46X	21.81	0.9516
600	1.71X	21.23	0.9508
500	2.05X	20.31	0.9495
400	2.56X	19.73	0.9485
300	3.41X	17.59	0.9437
200	5.12X	12.70	0.9160
100	10.2X	7.40	0.8086

Table 4 Summary of metrics for different compression ratios - B-scan

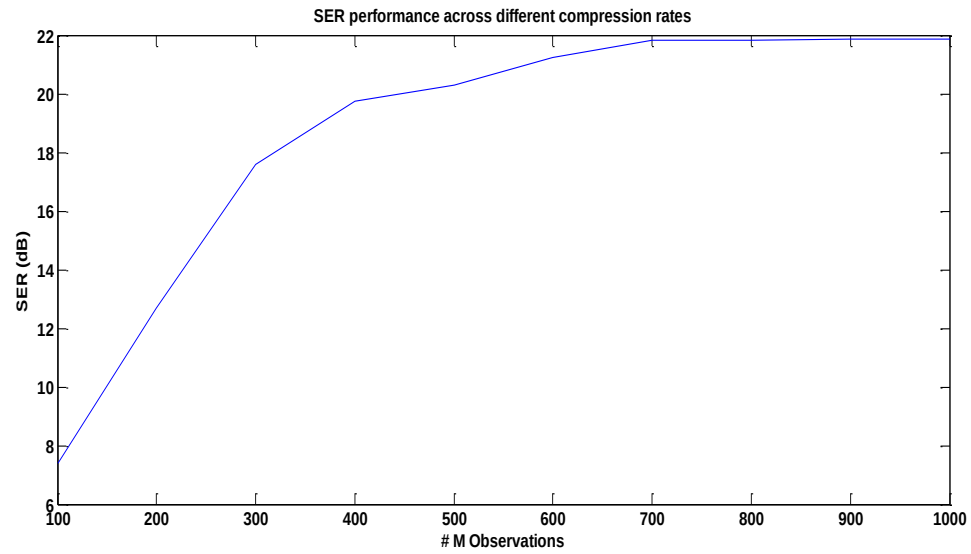

Figure 38 SER performance across compression rates - Single Rebar B-scan

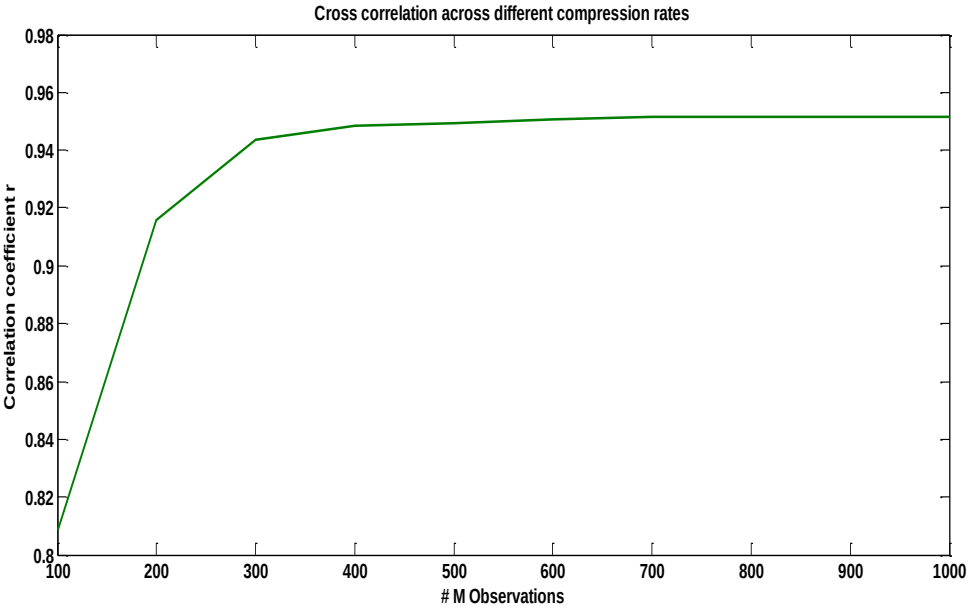

Figure 39 Cross correlation across compression rates - Single Rebar B-scan

3.4.4. B-scan Generation – Two Metal Rebars

To establish further validation for the proposed algorithm, a new channel, illustrated in Figure 40, was set up similar to the previous channel used with the addition of a second metal rebar as well.

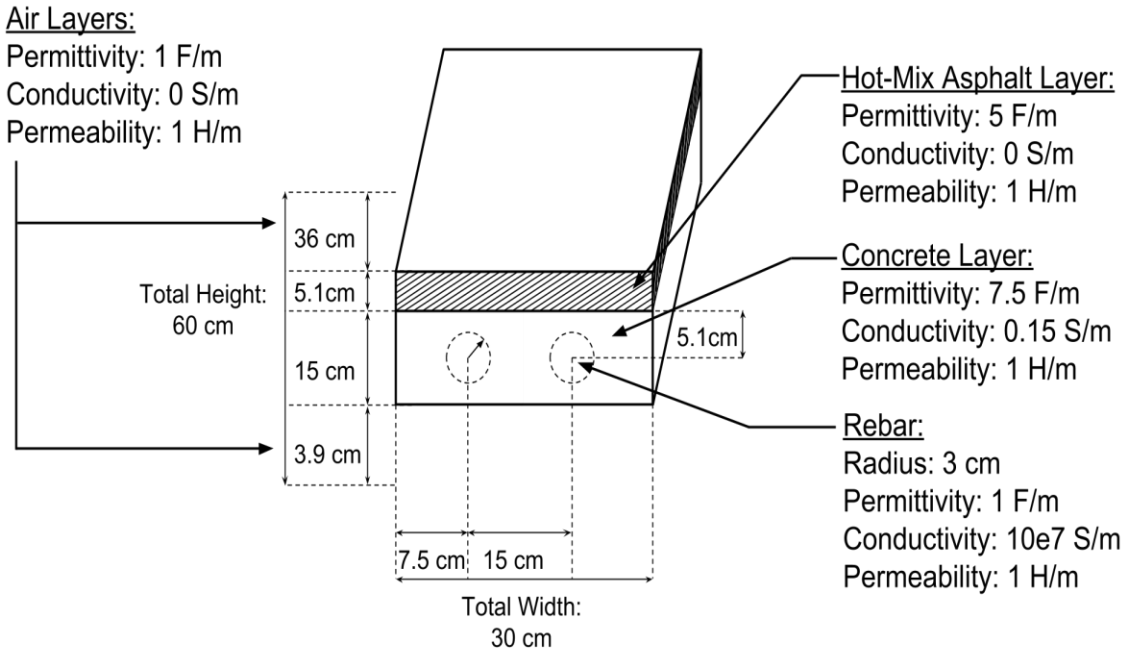

Figure 40 Detailed schematic describing channel parameters – Two Metal Rebars

The B-scans are generated for the same compression rate scenarios as mentioned above in section 3.4.4. The results are illustrated in the following figures and a summary is tabulated in Table 5.

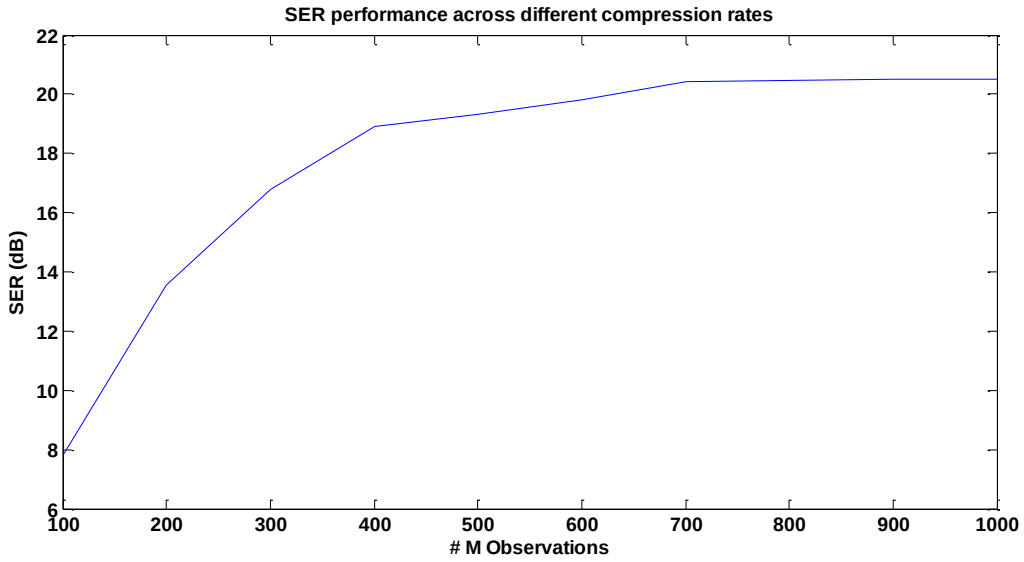

Figure 41 SER performance across compression rates - Two Rebars B-scan

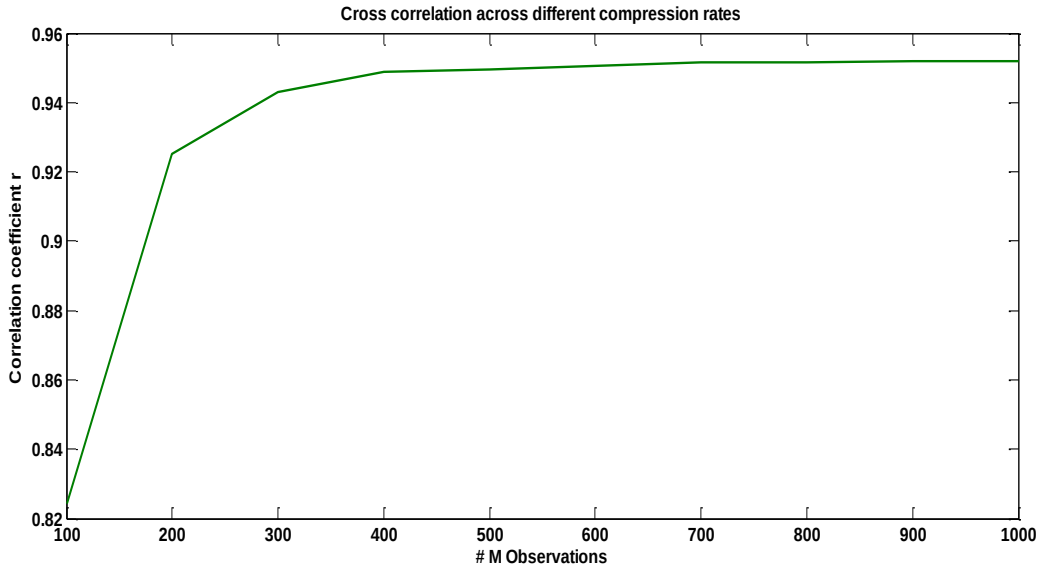

Figure 42 Cross correlation across compression rates - Two Rebars B-scan

M Observations	Compression Rate	SER (dB)	Correlation
1000	1.02X	20.50	0.9518
900	1.14X	20.49	0.9518
800	1.28X	20.46	0.9517
700	1.46X	20.42	0.9517
600	1.71X	19.73	0.9505
500	2.05X	19.31	0.9496
400	2.56X	18.90	0.9488
300	3.41X	16.78	0.9430
200	5.12X	13.55	0.9253
100	10.2X	7.84	0.8244

Table 5 Summary of metrics for different compression ratios - B-scan; Two Rebars

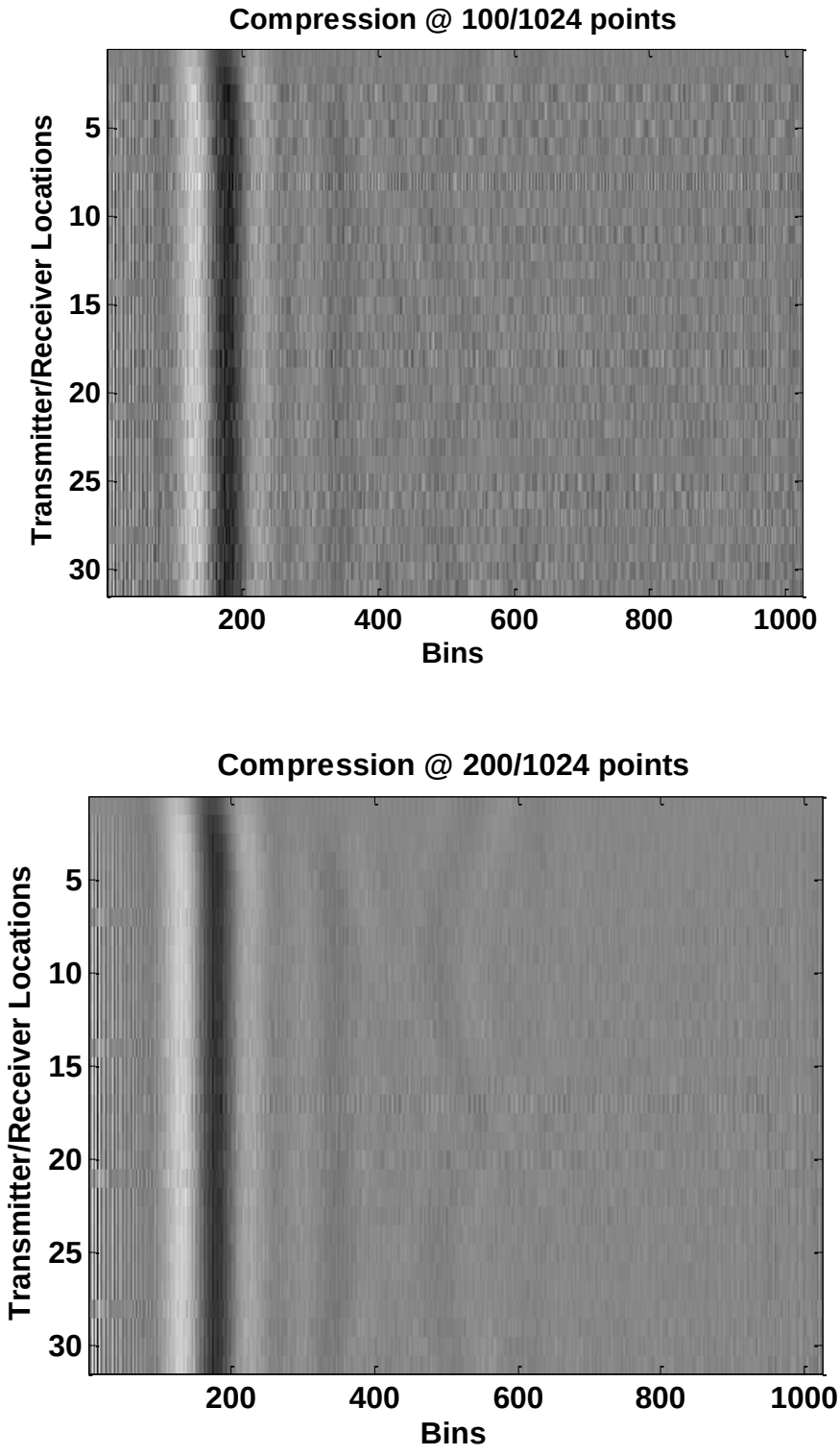

Figure 43 a) Reconstructed B-scan from 100 points b) Reconstructed B-scan from 200 points; Two Rebars

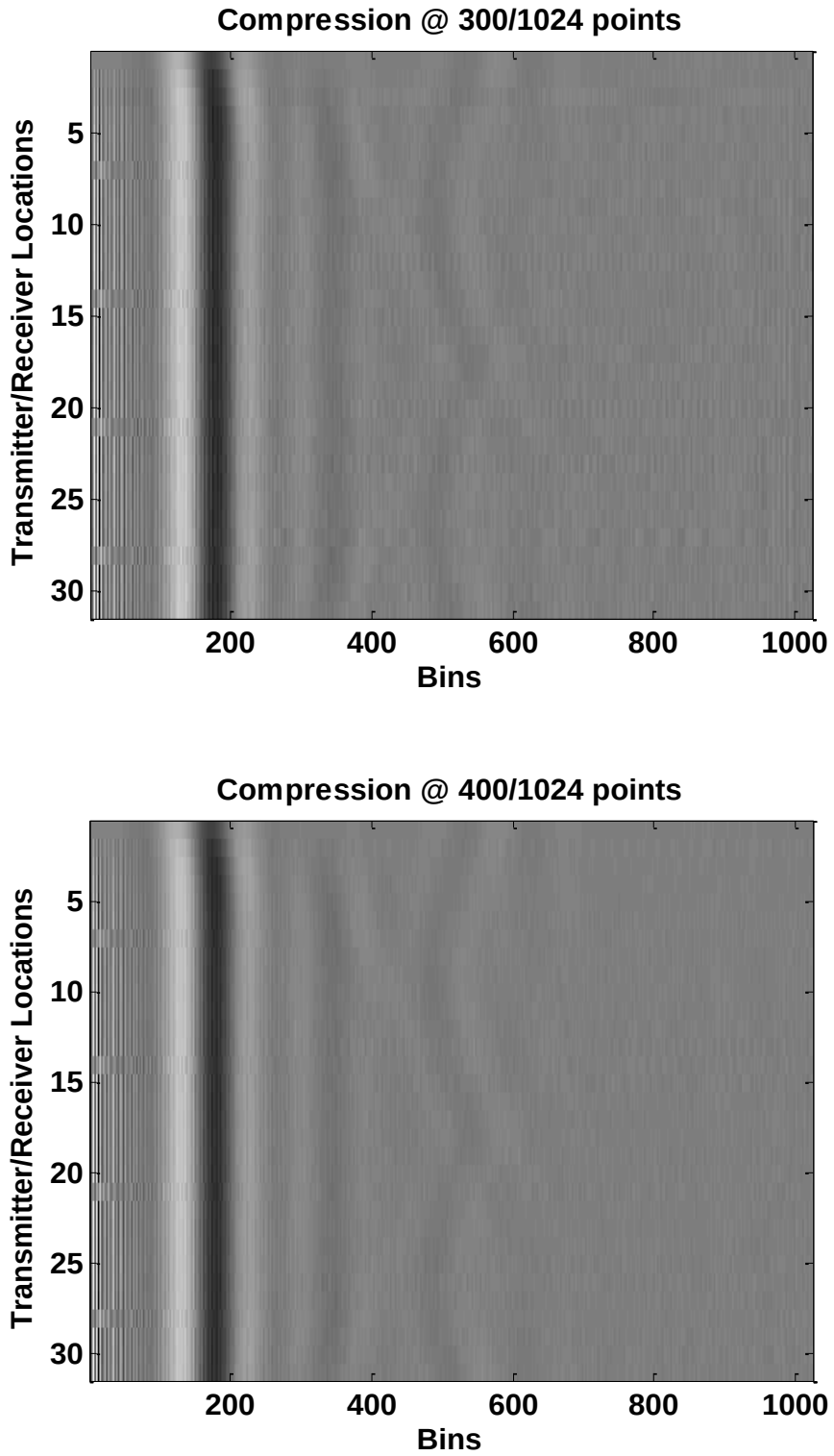

Figure 44 a) Reconstructed B-scan from 300 points b) Reconstructed B-scan from 400 points; Two Rebars

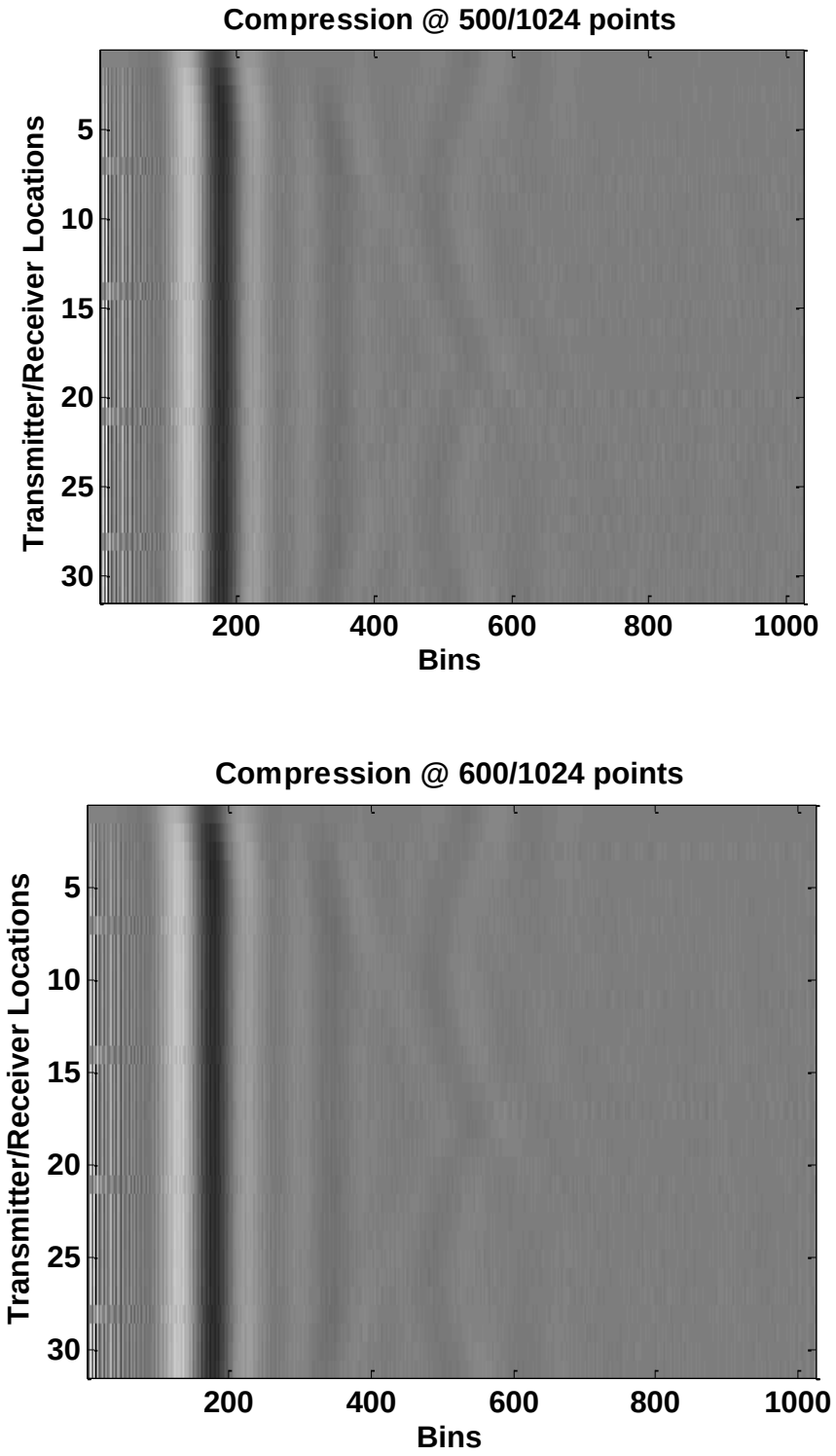

Figure 45 a) Reconstructed B-scan from 500 points b) Reconstructed B-scan from 600 points; Two Rebars

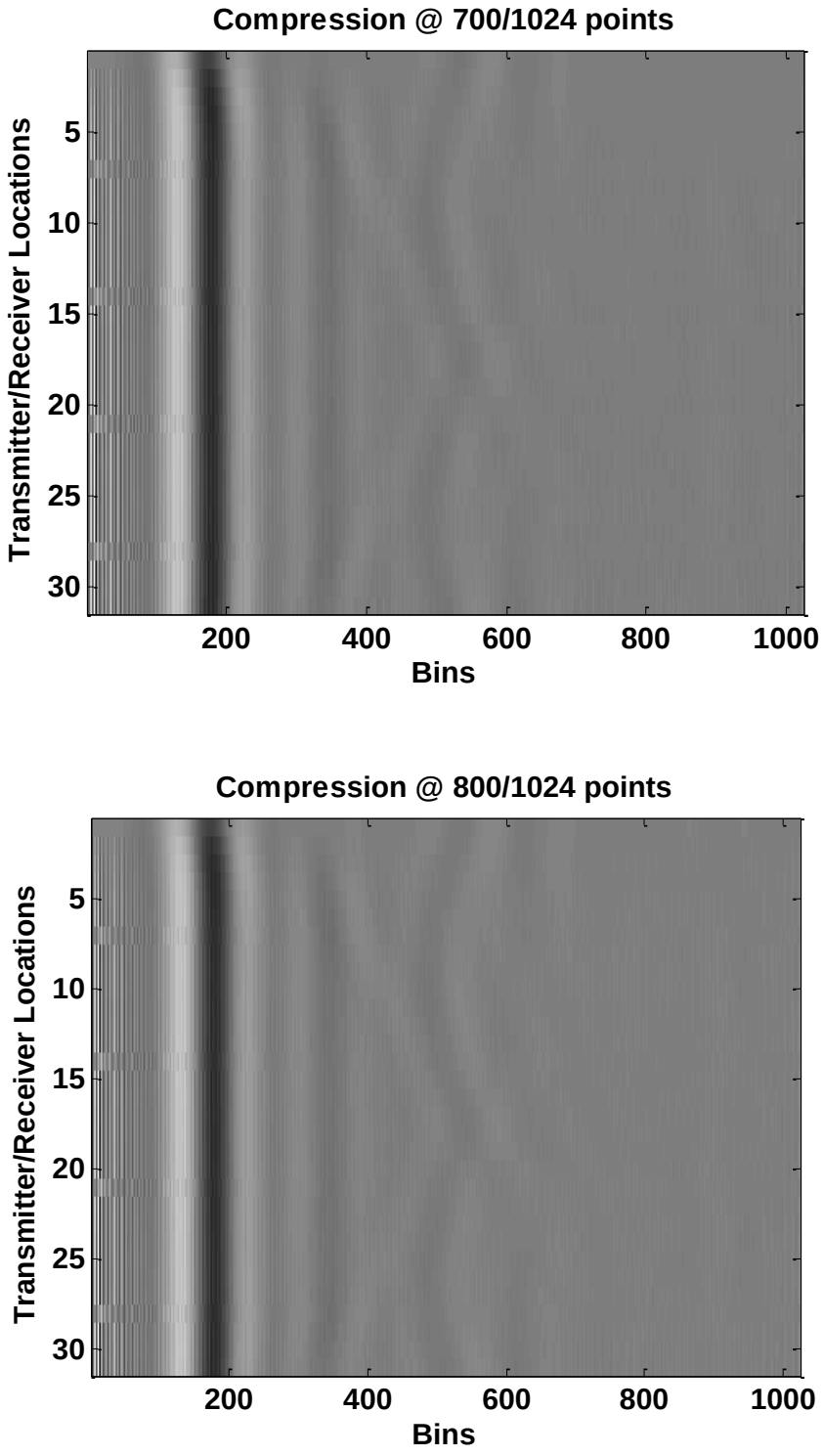

Figure 46 a) Reconstructed B-scan from 700 points b) Reconstructed B-scan from 800 points; Two Rebars

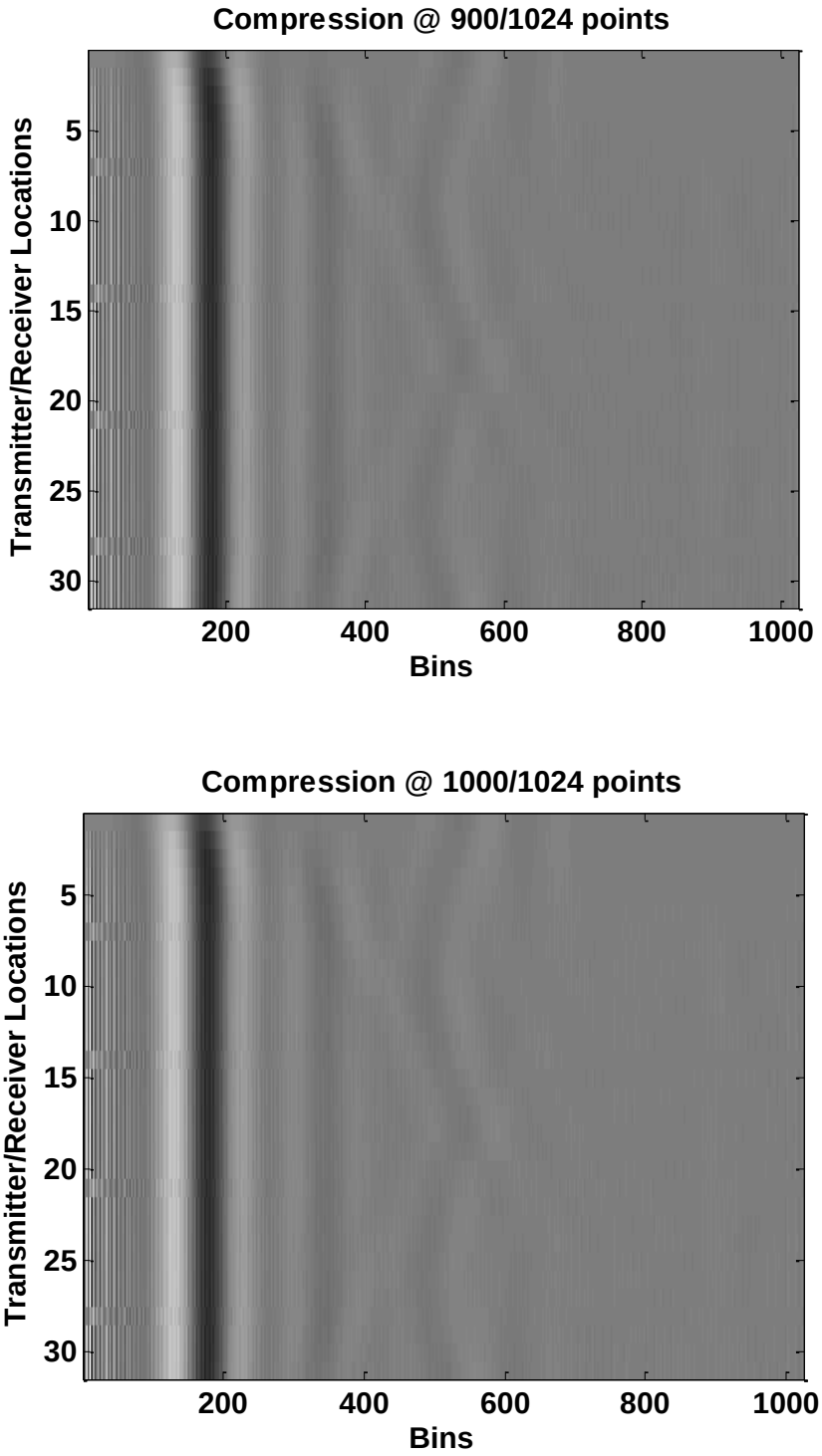

Figure 47 a) Reconstructed B-scan from 900 points b) Reconstructed B-scan from 1000 points; Two Rebars

3.6. Conclusion

I have presented a novel approach combining an OFDM-CS algorithm with existing SFCW GPR architecture. It is demonstrated that the system is able to achieve comparable results using only a fraction of the samples needed by the impulse system. In addition, this compressed fraction is sent out using multiple frequencies simultaneously to further reduce the scan time and effectively increasing the data acquisition speed. In order to compete with impulse radar systems, a frequency synthesizer whose settling time is on the order of microseconds would be the final step in realizing a compact hardware system that is cheaper than an impulse based GPR while performing comparably if not better. The question of whether the performance will exceed the impulse radar is what the future scope of work is going to be based on.

References

[1] Bettigole, N. and Robinson, R. (1997), Bridge Decks, American Society of Civil Engineers, New York.

[2] Uemori, S., Yamaguchi, T., Ito, S., Tan, Y., Kobayashi, H., Takai, N., Niitsu, K., and Ishikawa, N., "ADC linearity test signal generation algorithm," IEEE Asia Pacific Conference on Circuits and Systems, December 2010.

[3] Watanabe, K., Asami, K., Furukawa, Y., Ueda, M., Watanabe, T., Purtell, M. "WCDMA testing with a baseband IF range AWG," IEEE International Test Conference. 2002..

[4] Metwally, M., L'Esperance, N., Xia, T., Slamani M. (2013, November). Continuous Wave Radar Circuitry Testing Using OFDM Technique. IEEE 32nd VLSI Test Symposium.

[5] D. Donoho, "Compressed sensing," IEEE Trans. Inf. Theory, vol. 52, no. 4, pp. 1289–1306, Apr. 2006.

[6] E. Candes, J. Romberg, and T. Tao, "Robust uncertainty principles: Exact signal recovery from highly incomplete information," IEEE Trans. Inf. Theory, vol. 52, no. 2, pp. 489–509, Feb. 2006.

[7] E. Candes and J. Romberg, "Sparsity and incoherence in compressive sampling," Inv. Probl., vol. 23, no. 3, pp. 969–985, Jun. 2007.

[8] Ying, L., Zhang, Q., Hong, W., & YiRong, W. (2012). Waveform design and high-resolution imaging of cognitive radar based on compressive sensing. SCIENCE CHINA Information Sciences.

[9] Suksmono, A. B., Bharata, E., Lestari, A. A., Yarovoy, A. G., & Ligthart, L. P. (2010). *Compressive stepped-frequency continuous-wave ground-penetrating radar. Geoscience and Remote Sensing Letters, IEEE, 7(4),* 665-669.

[10] Sarkas, I. (2010). Step Frequency Radar Using Compressed Sensing. *Department of Mathematics of the University of Toronto, Tech. Rep.*

[11] Xia, T., Shetty, R., Platt, T., & Slamani, M. (2013). Low Cost Time Efficient Multi-tone Test Signal Generation Using OFDM Technique. Journal of Electronic Testing, 29(6), 893-901

[12] Xia, T. "Techniques to leverage test speed of wide band circuit/system-multitone sign generation and characterization," IEEE VLSI Test Symposium (VTS)'13 Elevator Talk.

[13] A. Langman and M. Inggs: "Pulse versus stepped frequency continuous wave modulation for ground penetrating radar", IGARSS Geoscience and Remote Sensing Symposium, pp. 1533-1535, 2001.

[14] Ziani, T., Laour, M., Dérobert, X., & Benslama, M. (2009, September). 2 D simulation with the FDTD method of GPR modelling applied to the detection in stratified lossy medium using the frequency effect pulse. In *Electromagnetics in Advanced Applications, 2009. ICEAA'09. International Conference on* (pp. 20-23). IEEE.

[15] Taflove, A., & Brodwin, M. E. (1975). Numerical solution of steady-state electromagnetic scattering problems using the time-dependent Maxwell's equations. *Microwave Theory and Techniques, IEEE Transactions on*, *23*(8), 623-630.

CHAPTER 4: COMPREHENSIVE CONCLUSION AND FUTURE SCOPE OF WORK

The OFDM coupled compressive algorithm presented in this work was motivated by the need to offer a new solution to the data acquisition speed problem faced by SFCW. This chapter summarizes the main ideas presented in the thesis and recommends future research directions.

4.1. Conclusions

- SFCW is able to achieve the same range resolution as the impulse radar using the relationship between the range resolution and the frequency step size and bandwidth utilized.
- SFCW architecture is capable of achieving a much higher dynamic range when compared with the impulse radar.
- OFDM section of the proposed method contributes to the reduction of scan time or increasing the data acquisition speed, through multi-tone signal transmission.
- Compressive sampling contributes on two fronts. The first is in the reduction of scan time by compressing the transmit signal, effectively reducing the number of frequencies to be transmitted. The second front is the overall mean radiated power is reduced due to the reduction in frequencies being transmitted.
- Continuous wave radar is capable of pushing more power per tone when compared against impulse radar.

- OFDM coupled compressive algorithm was verified using a simple channel with ideal parameters and using a realistic bridge deck model for added validation.
- With compression set to 50%, the ideal channel's A-scan achieved an SER of 39.1 dB and a correlation of 0.9999. Similarly, the realistic channel's A-scan with single rebar achieved an SER of 25.3 dB and a correlation of 0.9986.
- Furthermore, with compression set to 50%, the single rebar B-scan achieved an SER of 20.31 dB and a correlation of 0.9495. Similarly, the two rebar B-scan achieved an SER of 19.31 dB and a correlation of 0.9496.

4.2. Future Work

The research has shown sufficient results to conclude that the OFDM coupled compressive algorithm can improve SFCW's data acquisition speed to compete with that of the impulse radar system. In addition, SFCW's high dynamic range and higher power per tone capabilities, make the proposed system a formidable adversary to the commercially favored impulse radar system. However, a few questions remain unanswered, paving the way for the future research direction.

- Researching the actual reduction in the amount of time needed for data acquisition using the OFDM-CS SFCW architecture by implementing it onto hardware. The hardware comprising of an FPGA and a high-speed DAC would be needed to replicate the simulations and further validate them in a lab setting.
- Based on hardware experiments, approximations can be calculated to further test the architecture and assess whether its performance can surpass the impulse radar.

COMPREHENSIVE BIBLIOGRAPHY

[1] Bettigole, N. and Robinson, R. (1997), Bridge Decks, American Society of Civil Engineers, New York.

[2] D . J .Daniels, Surface Penertating Radar, London, IEEE, c1996

[3] D. A. Noon, Stepped-Frequency Radar Design and Signal Processing Enhances Ground Penetrating Radar Performance, Dept. of Electrical & Computer Eng., University of Queensland and Cooperative Research Centre for Sensor Signal and Information Processing, January 1996

[4] Fowler, C., Entzminger, J., & Corum, J. (1990). Assessment of ultra-wideband(UWB) technology. IEEE Aerospace and Electronic Systems Magazine, 5(11), 45-49.

[5] Kahimbaara, G. M. (2004). Investigation and Simulation of an Impulse Ground Penetrating Radar Application (Doctoral dissertation, BSc. Thesis, University of Cape Town).David Daniels, ed: Ground Penetrating Radar, 2nd ed, The Institution of Electrical Engineers, London, United Kingdom, 2004.

[6] A. Langman and M. Inggs: "Pulse versus stepped frequency continuous wave modulation for ground penetrating radar", IGARSS Geoscience and Remote Sensing Symposium, pp. 1533-1535, 2001.

[7] Weiss, J. M. Continuous-Wave Stepped-Frequency Radar for Target Ranging and Motion Detection.

[8] Scheers, B. (2001). Ultra-wideband ground penetrating radar with application to the detection of anti personnel landmines. Chapter, 7, 867-871.

[9] Mandalanka, A. K. (2013). UWB pulse generation for GPR applications(Doctoral dissertation).

[10] Loulizi, A. (2001). Development of ground penetrating radar signal modeling and implementation for transportation infrastructure assessment (Doctoral dissertation, Virginia Polytechnic Institute and State University).

[11] Sylla, I. T., "Building an RF source for low cost testers using an ADPLL controlled by Texas Instruments digital signal processor DSP TMS320C5402," IEEE International Test Conference, November 2003.

[12] Lu, A.K., Roberts, G..,"An oversampling-based analog multitone signal generator," Circuits and Systems II: Analog and Digital Signal Processing, IEEE Transactions 45, 391–394. 1998.

[13] Uemori, S., Yamaguchi, T., Ito, S., Tan, Y., Kobayashi, H., Takai, N., Niitsu, K., and Ishikawa, N., "ADC linearity test signal generation algorithm," IEEE Asia Pacific Conference on Circuits and Systems, December 2010.

[14] Watanabe, K., Asami, K., Furukawa, Y., Ueda, M., Watanabe, T., Purtell, M. "WCDMA testing with a baseband IF range AWG," IEEE International Test Conference. 2002..

[15] Metwally, M., L'Esperance, N., Xia, T., Slamani M. (2013, November). Continuous Wave Radar Circuitry Testing Using OFDM Technique. IEEE 32nd VLSI Test Symposium.

[16] Xia, T., Shetty, R., Platt, T., & Slamani, M. (2013). Low Cost Time Efficient Multi-tone Test Signal Generation Using OFDM Technique. Journal of Electronic Testing, 29(6), 893-901

[17] Xia, T. "Techniques to leverage test speed of wide band circuit/system-multitone sign generation and characterization," IEEE VLSI Test Symposium (VTS)'13 Elevator Talk.

[18] D. Donoho, "Compressed sensing," IEEE Trans. Inf. Theory, vol. 52, no. 4, pp. 1289–1306, Apr. 2006.

[19] E. Candes, J. Romberg, and T. Tao, "Robust uncertainty principles: Exact signal recovery from highly incomplete information," IEEE Trans. Inf. Theory, vol. 52, no. 2, pp. 489–509, Feb. 2006.

[20] E. Candes and J. Romberg, "Sparsity and incoherence in compressive sampling," Inv. Probl., vol. 23, no. 3, pp. 969–985, Jun. 2007.

[21] Ying, L., Zhang, Q., Hong, W., & YiRong, W. (2012). Waveform design and high-resolution imaging of cognitive radar based on compressive sensing. SCIENCE CHINA Information Sciences.

[22] Suksmono, A. B., Bharata, E., Lestari, A. A., Yarovoy, A. G., & Ligthart, L. P. (2010). *Compressive stepped-frequency continuous-wave ground-penetrating radar*. *Geoscience and Remote Sensing Letters, IEEE, 7(4),* 665-669.

[23] Sarkas, I. (2010). Step Frequency Radar Using Compressed Sensing. *Department of Mathematics of the University of Toronto, Tech. Rep.*

[24] Mahafza, B.R. 2000. “Radar systems analysis and design using Matlab,” Chapman & Hall/CRC, Boca Raton.

[25] Ziani, T., Laour, M., Dérobert, X., & Benslama, M. (2009, September). 2 D simulation with the FDTD method of GPR modelling applied to the detection in stratified lossy medium using the frequency effect pulse. In *Electromagnetics in Advanced Applications, 2009. ICEAA'09. International Conference on* (pp. 20-23). IEEE.

[26] Taflove, A., & Brodwin, M. E. (1975). Numerical solution of steady-state electromagnetic scattering problems using the time-dependent Maxwell's equations. *Microwave Theory and Techniques, IEEE Transactions on*, *23*(8), 623-630.